# Toroidalne izomery w najcięższych jądrach atomowych

*Andrzej Staszczak*

UMCS
UNIWERSYTET MARII CURIE-SKŁODOWSKIEJ
W LUBLINIE

KATEDRA FIZYKI TEORETYCZNEJ
UMCS LUBLIN

**SEMINARIUM FIZYKI JĄDRA ATOMOWEGO**

*Warszawa, 15.11.2018 r.*

# Bimodal fission in $^{306}122$: symmetric elongated (sEF) and asymmetric (aEF)

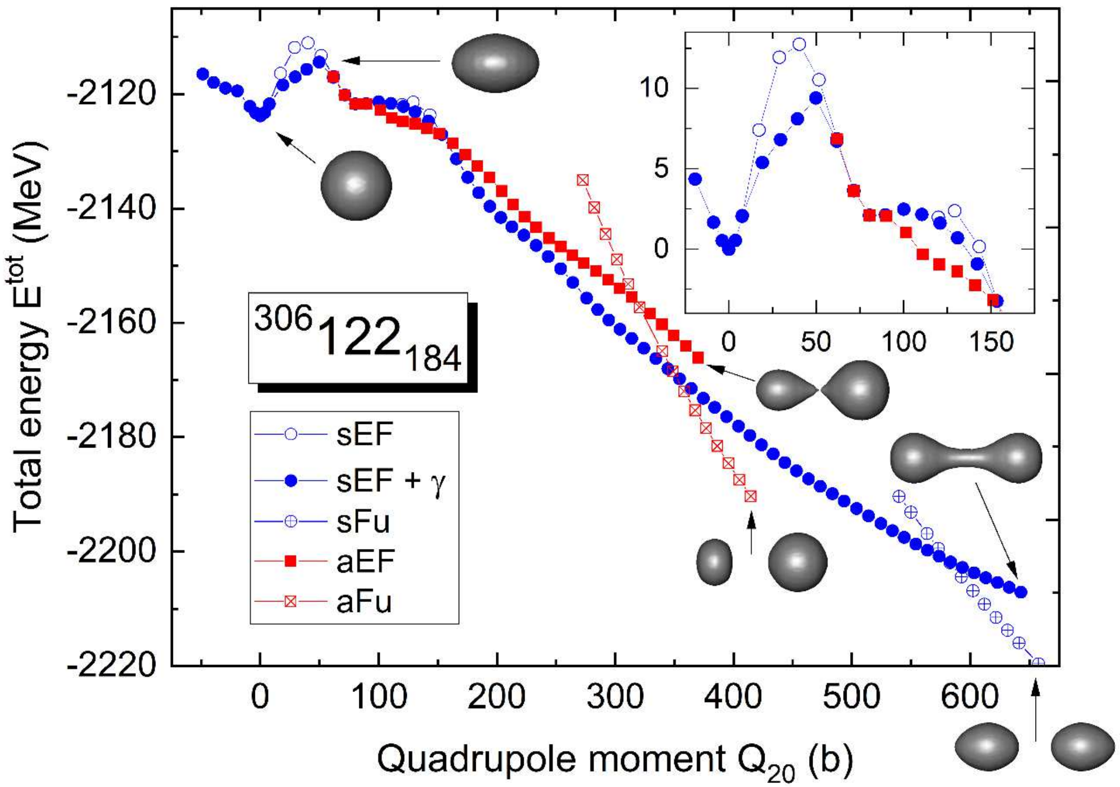


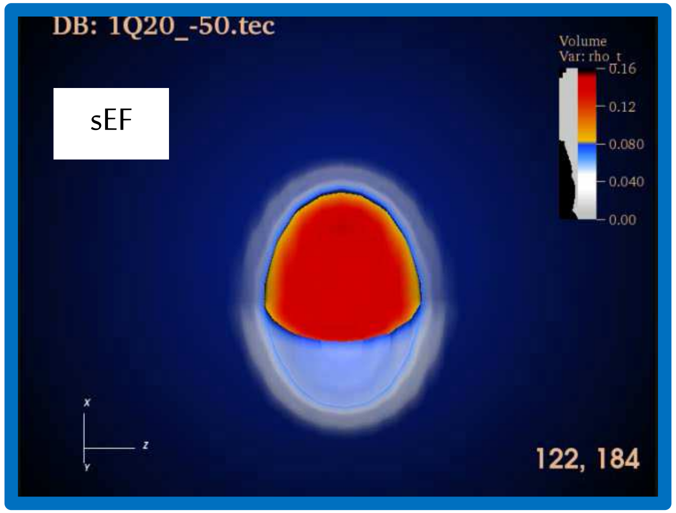


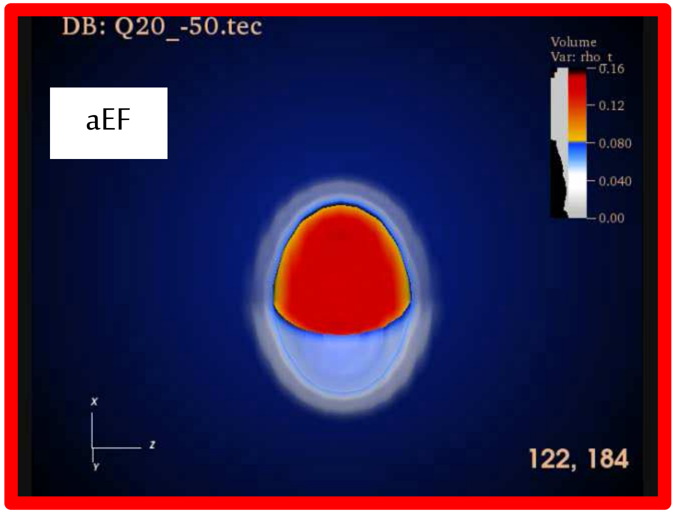

# Bimodal fission in $^{304}120$:
# symmetric elongated (sEF) and asymmetric (aEF)

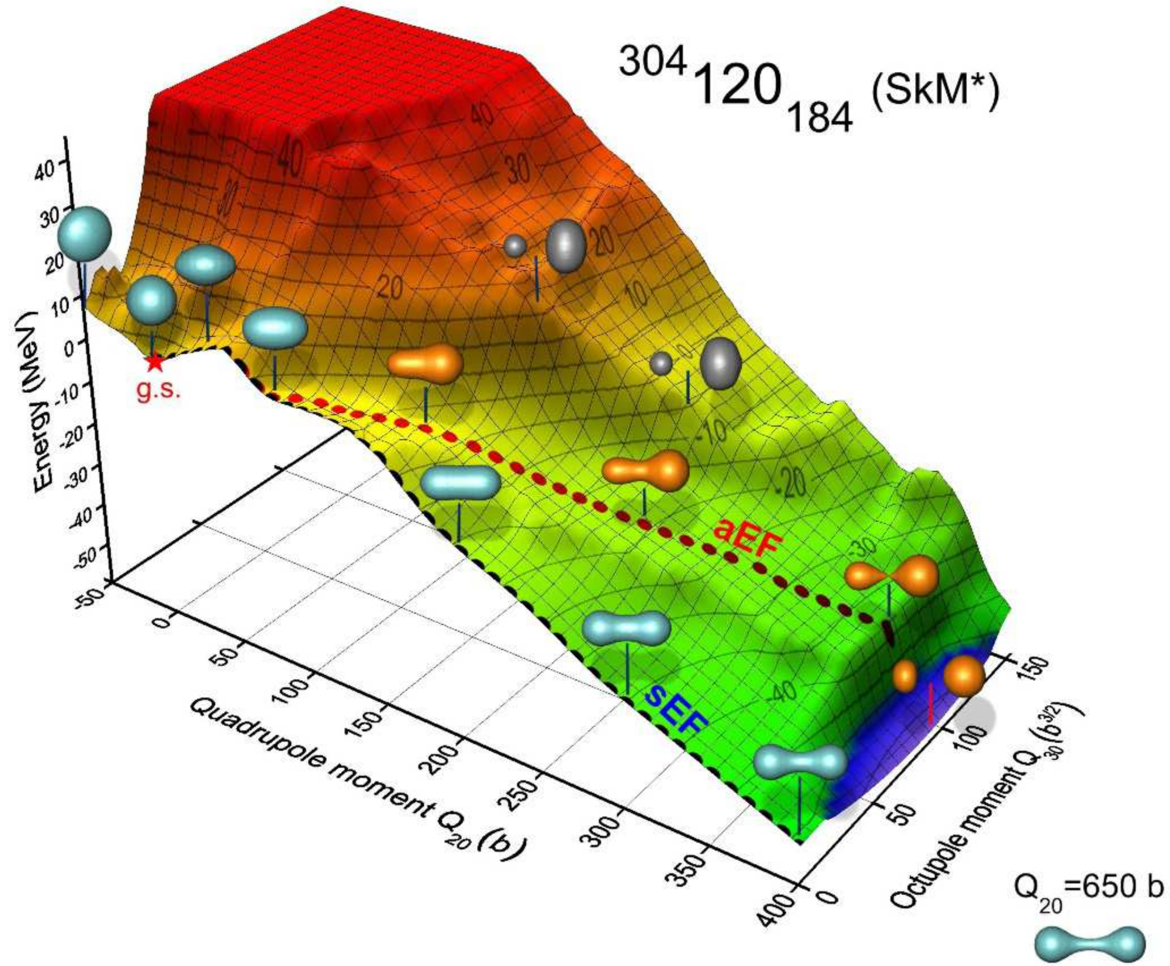

# Bimodal fission in $^{304}$120:
# symmetric elongated (sEF) and asymmetric (aEF)

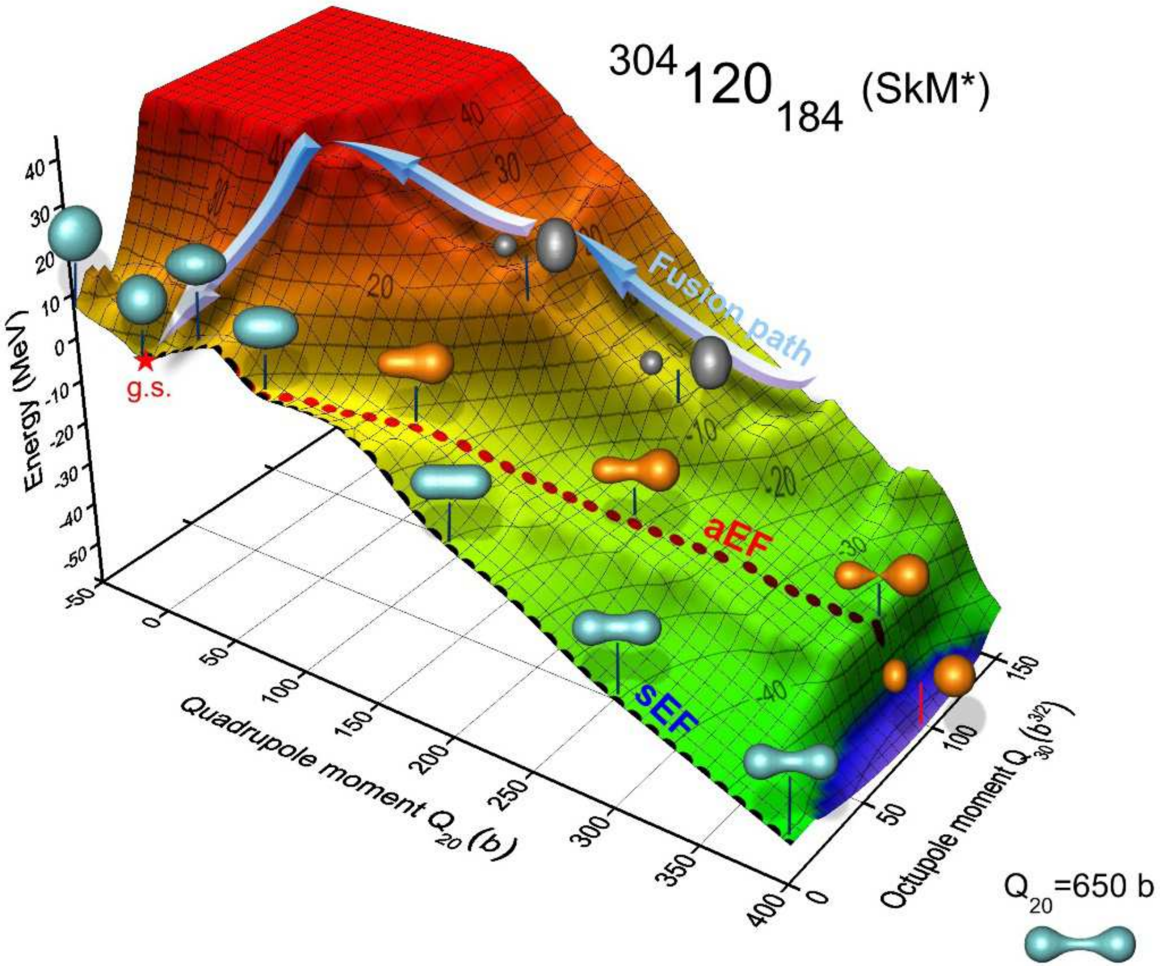

# Bimodal fission in $^{304}120$: symmetric elongated (sEF) and asymmetric (aEF)

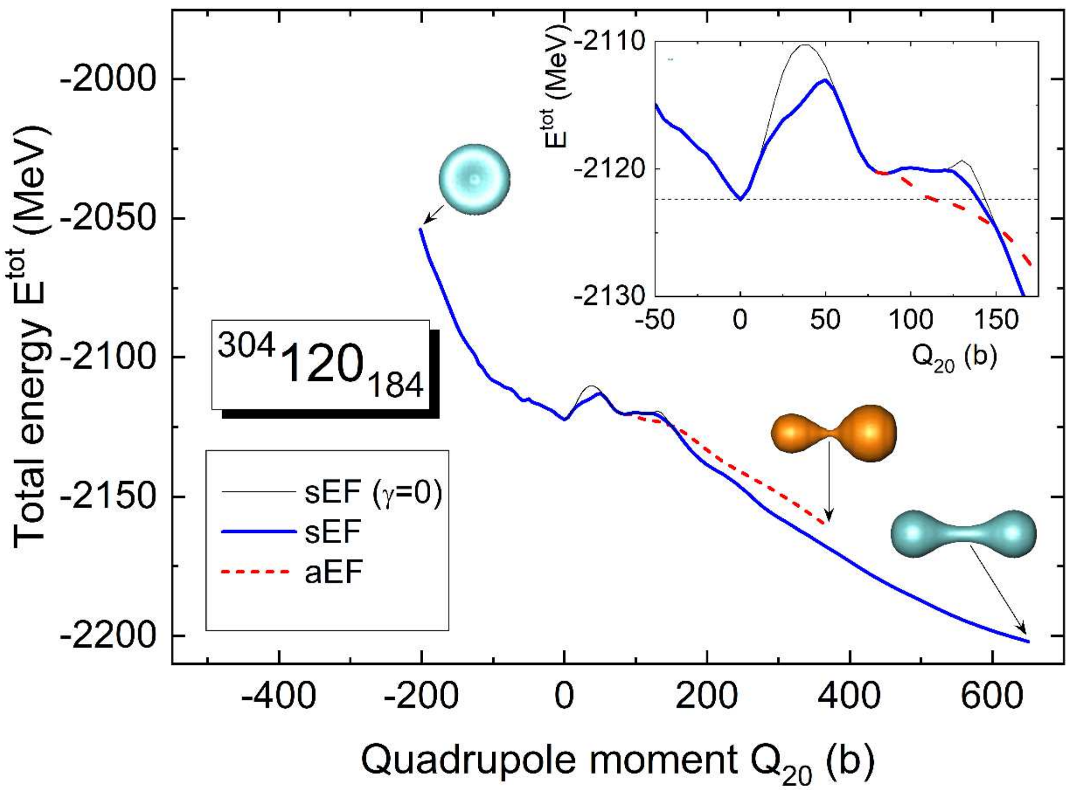

# Shape transition from a biconcave disc to torus in $^{304}120$

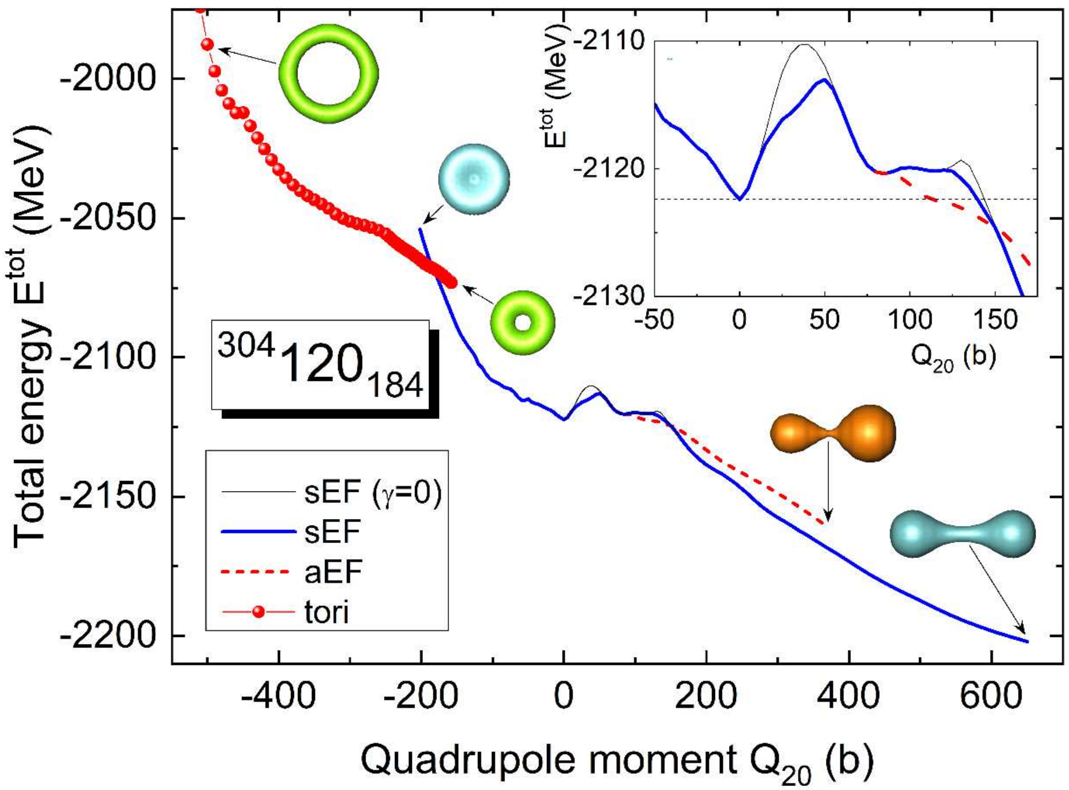


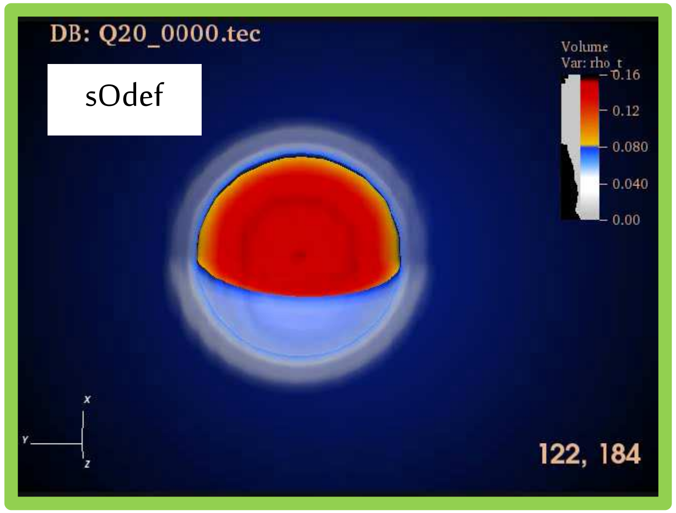

# Shape transition from a biconcave disc to a torus in $^{304}120$

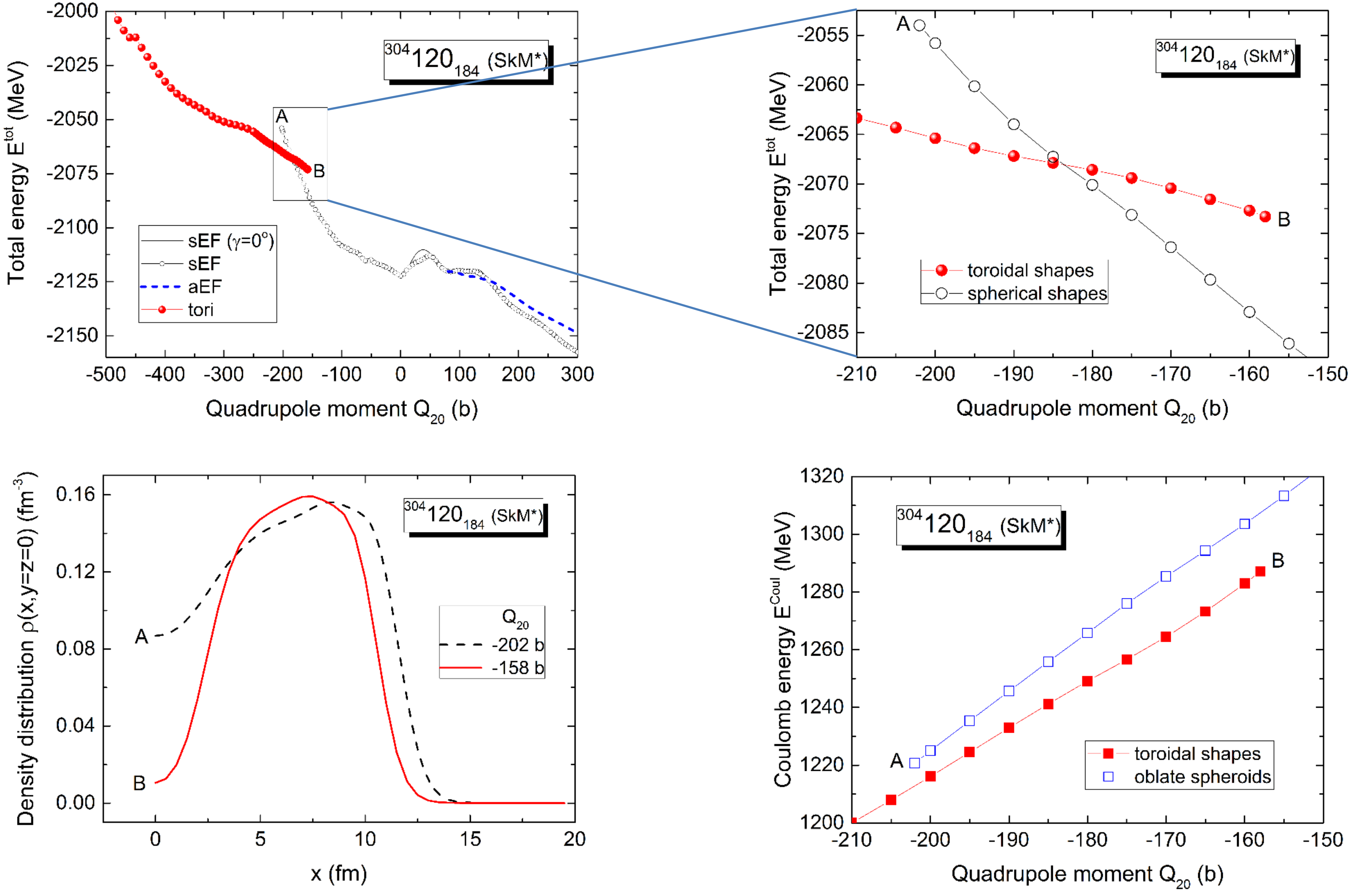

# Shape transition from a biconcave disc to a torus in $^{304}120$

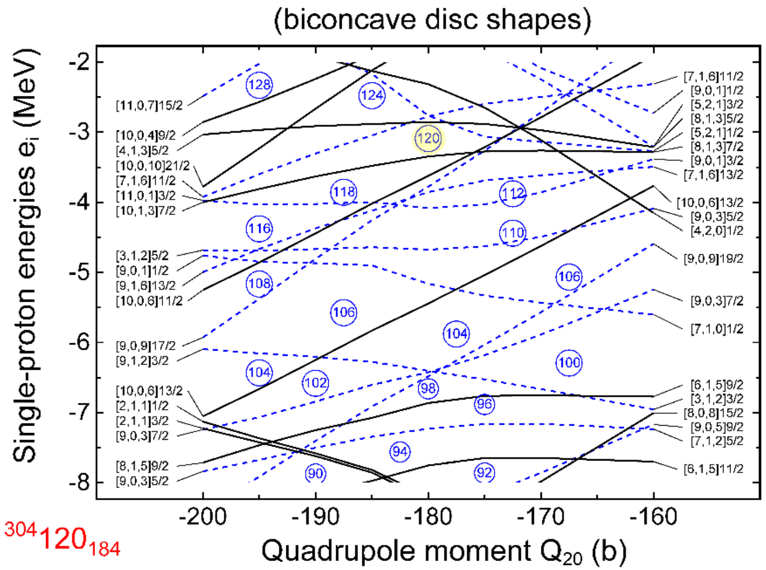


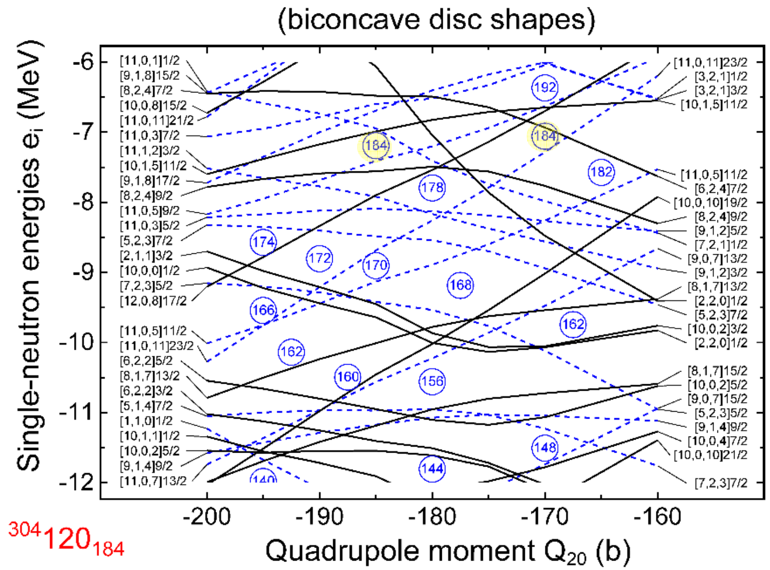


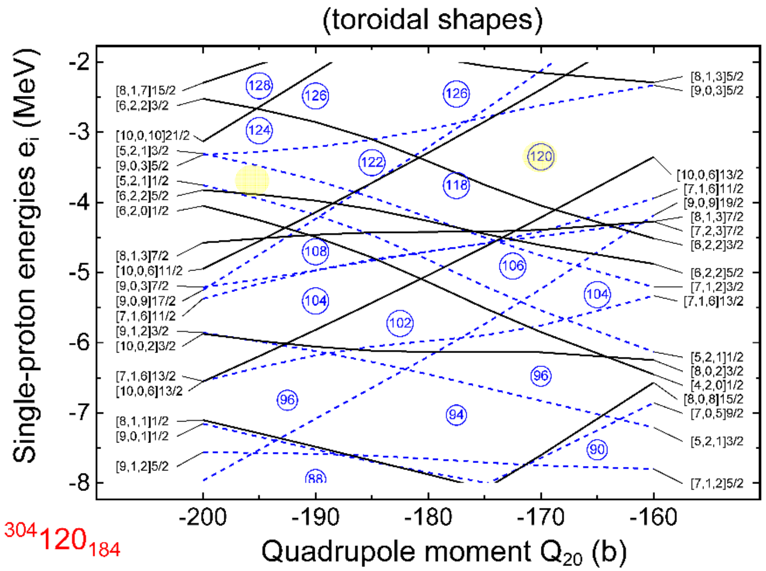


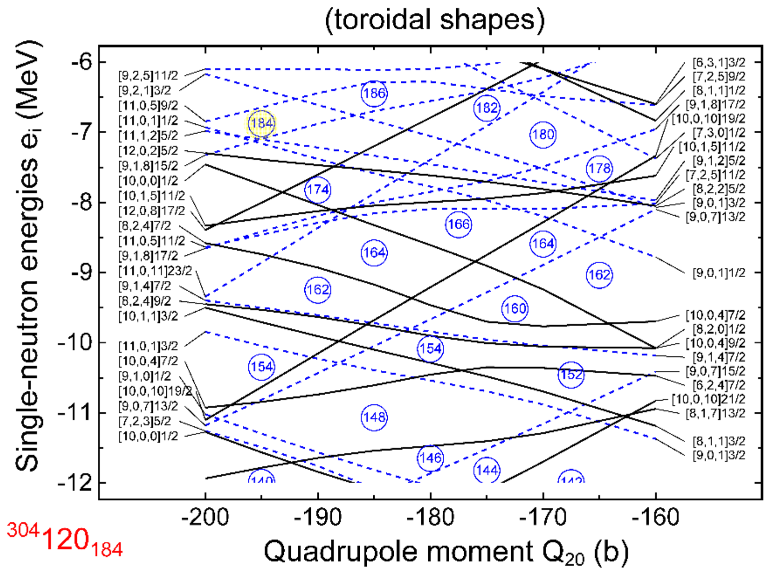

# Shape transition from a biconcave disc to a torus for e-e isotopes $Z$=120 and isotones $N$=184

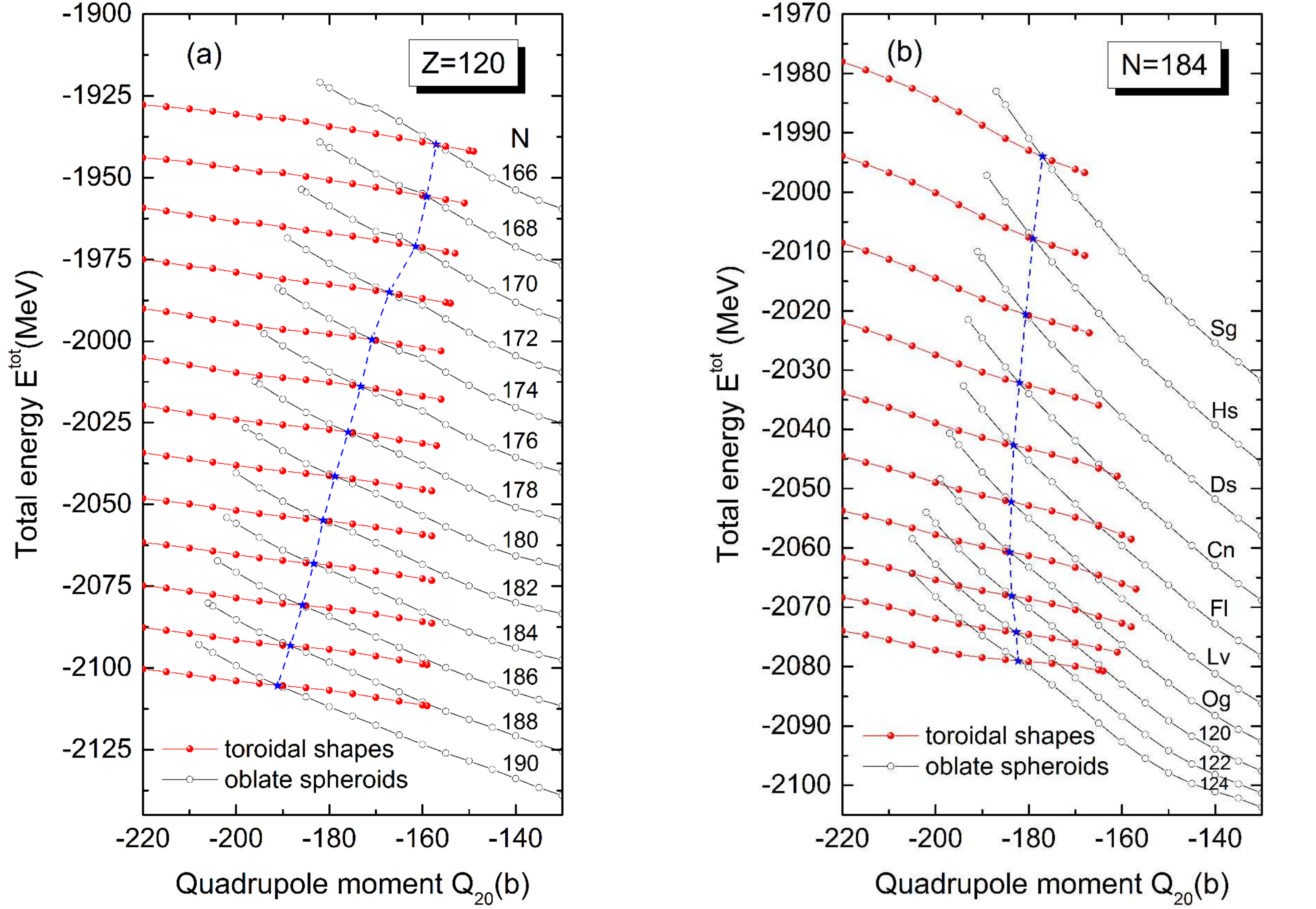


Phase coexistence – first-order phase transition

# Toroidal high-spin isomers (THSI) in $^{304}120$

Single-particle levels in the canonical basis as a function of $Q_{20}$

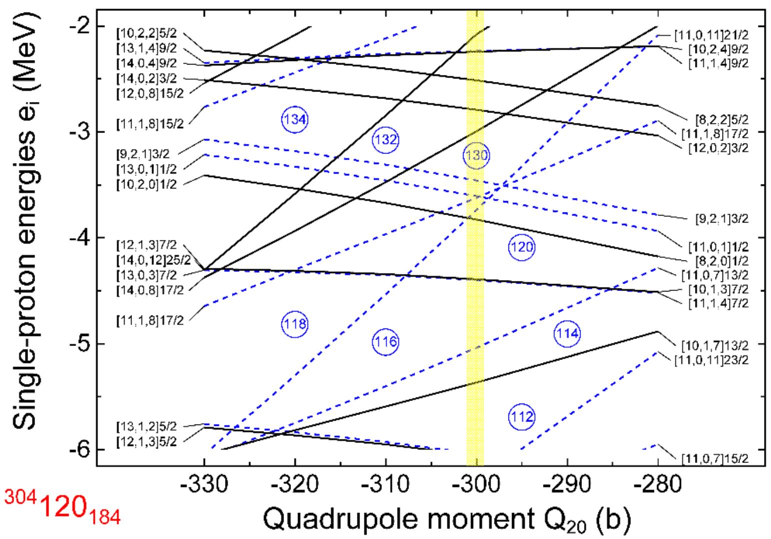


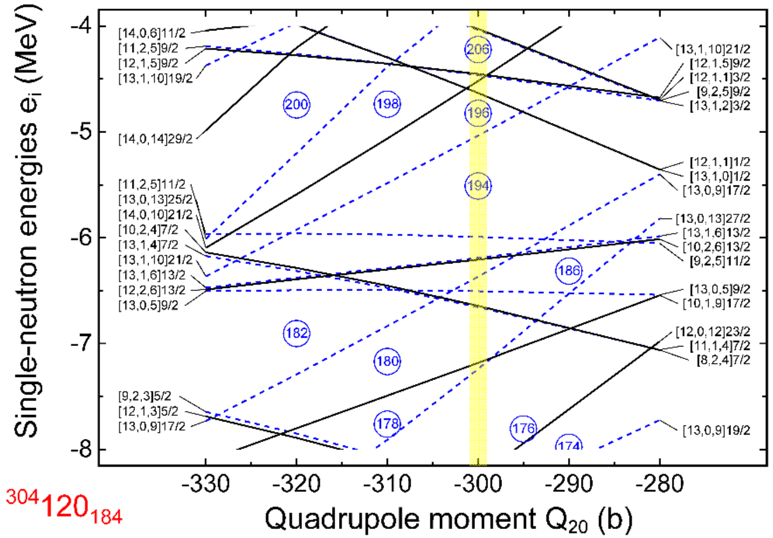


Single-particle levels in the canonical basis as a function of $\Omega_z$

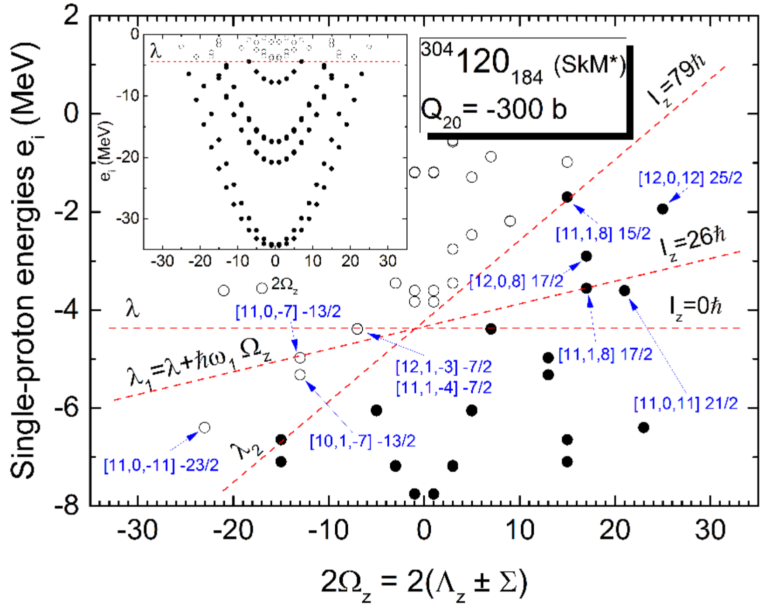


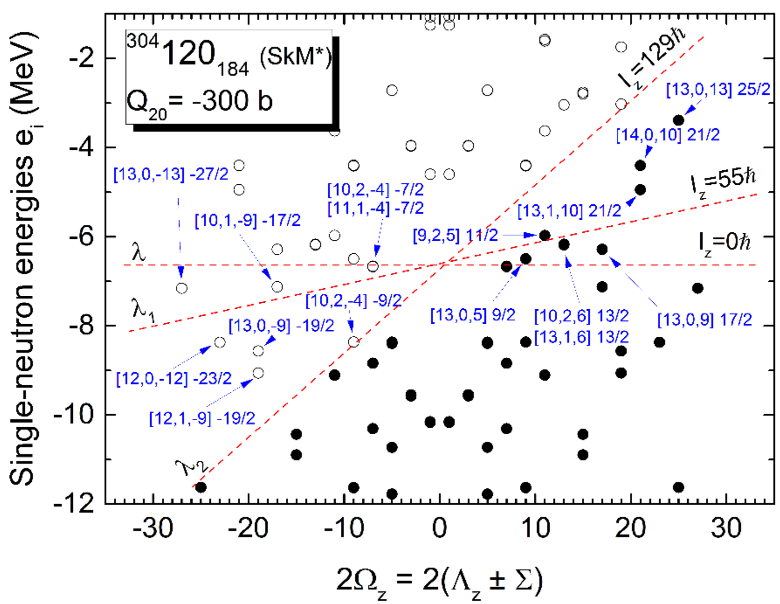

# Toroidal high-spin isomers (THSI) in $^{304}120$

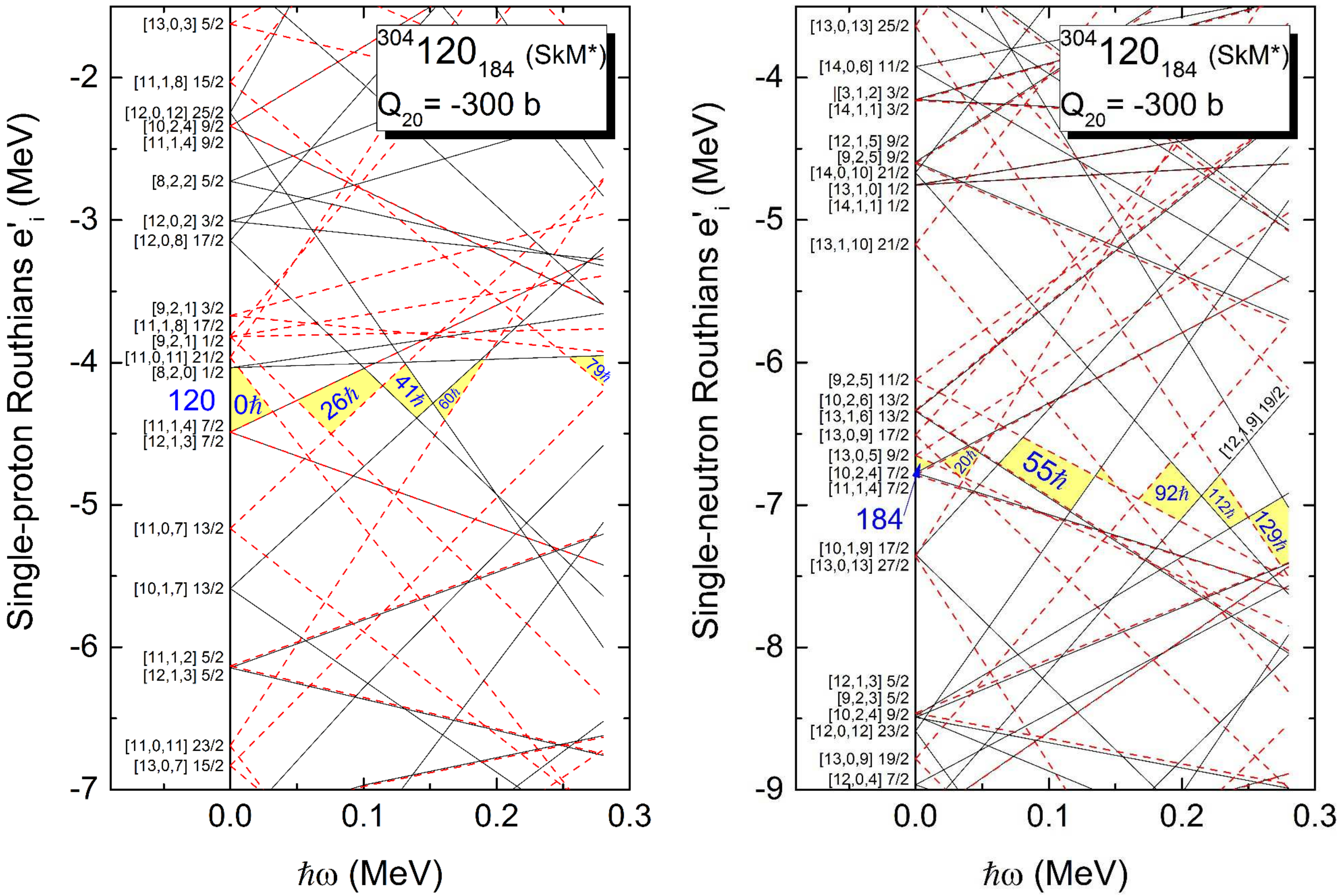


Single-particle Routhians as a function of the cranking frequency $\hbar\omega$

# Toroidal high-spin isomers (THSI) in $^{304}120$

PHYSICAL REVIEW C **95**, 054315 (2017)

TABLE I. The particle-hole excitation configurations leading to the states of $^{304}120_{184}$ with $I_z = I_z(\text{proton}) + I_z(\text{neutron}) = 26 + 55 = 81$ and $I_z = 79 + 129 = 208$.

| | Hole states | Particle states |
|---|---|---|
| | [11,1,−4] −7/2 | [11,0,11] 21/2 |
| $I_z$(proton) = 26 | [12,1,−3] −7/2 | [11,1,8] 17/2 |
| | [11,0,−7] −13/2 | [12,0,8] 17/2 |
| | [10,1,−7] −13/2 | [12,0,12] 25/2 |
| $I_z$(proton) = 79 | [11,0,−11] −23/2 | [11,1,8] 15/2 |
| | [10,2,−4] −7/2 | [13,0,5] 9/2 |
| | [11,1,−4] −7/2 | [13,0,9] 17/2 |
| | [10,1, 9] 17/2 | [13,1,6] 13/2 |
| $I_z$(neutron) = 55 | [13,0,−13] −27/2 | [10,2,6] 13/2 |
| | [12,0,−12] −23/2 | [9,2,5] 11/2 |
| | [13,0,−9] −19/2 | [13,1,10] 21/2 |
| | [12,1,−9] −19/2 | [14,0,10] 21/2 |
| $I_z$(neutron) = 129 | [10,2,−4] −9/2 | [13,0,13] 25/2 |

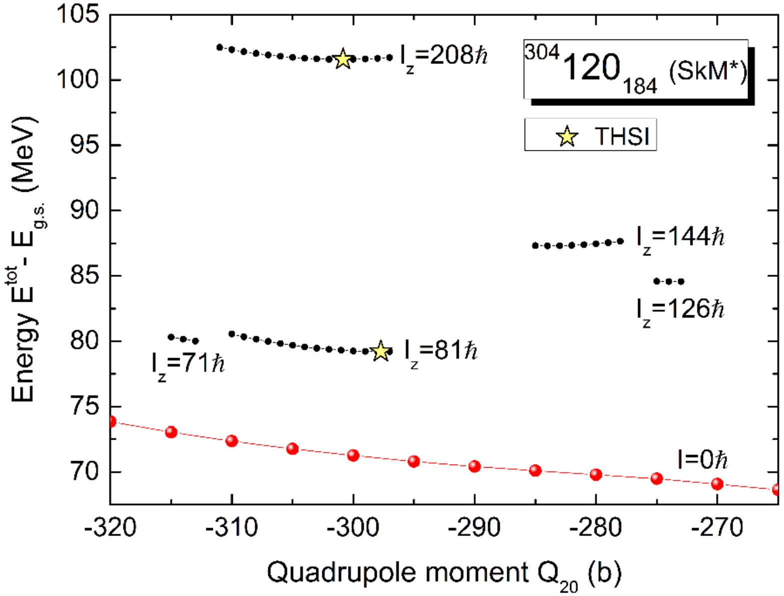


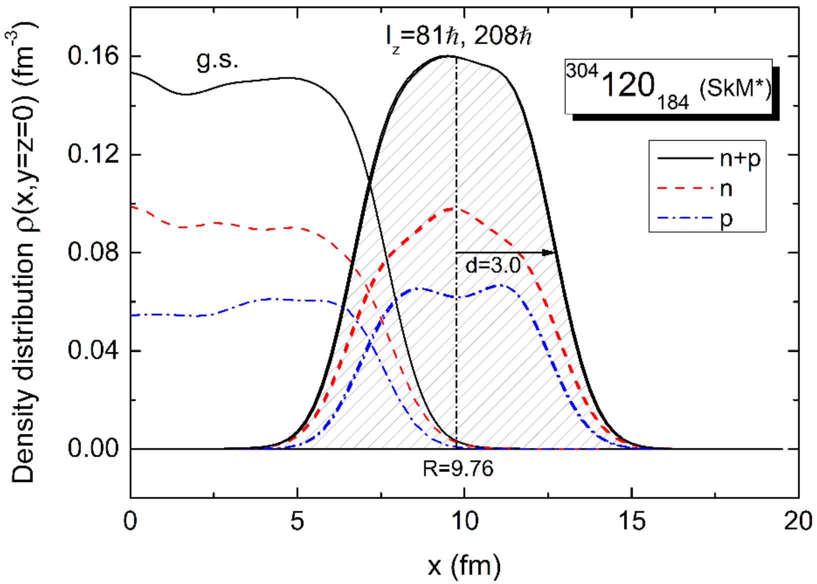


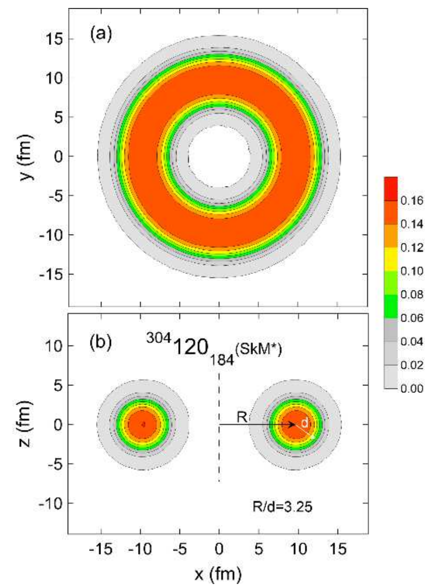

# Hiper-heavy isotones $N$=196

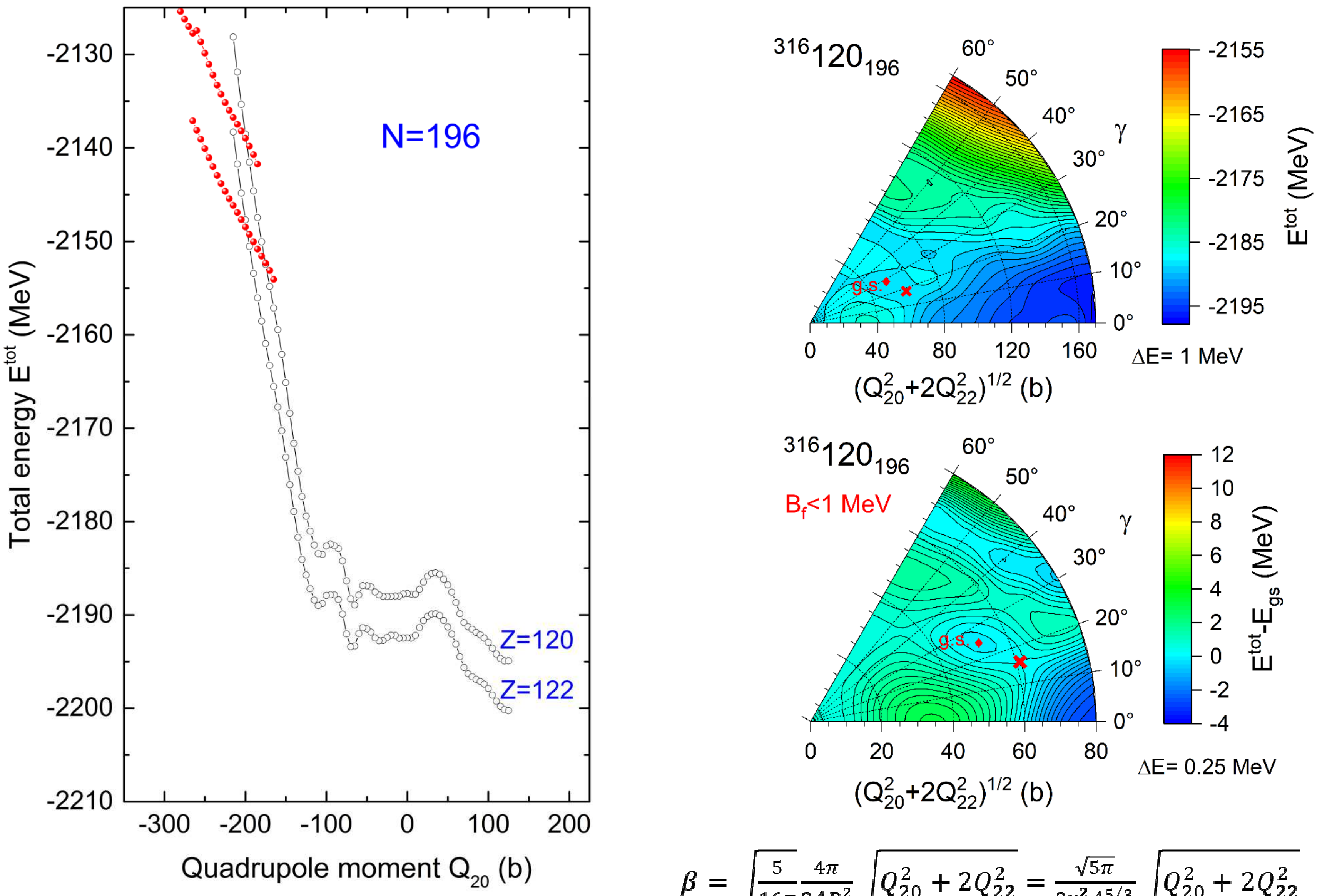


$$\beta = \sqrt{\frac{5}{16\pi}}\frac{4\pi}{3AR_0^2}\sqrt{Q_{20}^2 + 2Q_{22}^2} = \frac{\sqrt{5\pi}}{3r_0^2 A^{5/3}}\sqrt{Q_{20}^2 + 2Q_{22}^2}$$

# Hiper-heavy isotones $N$=196

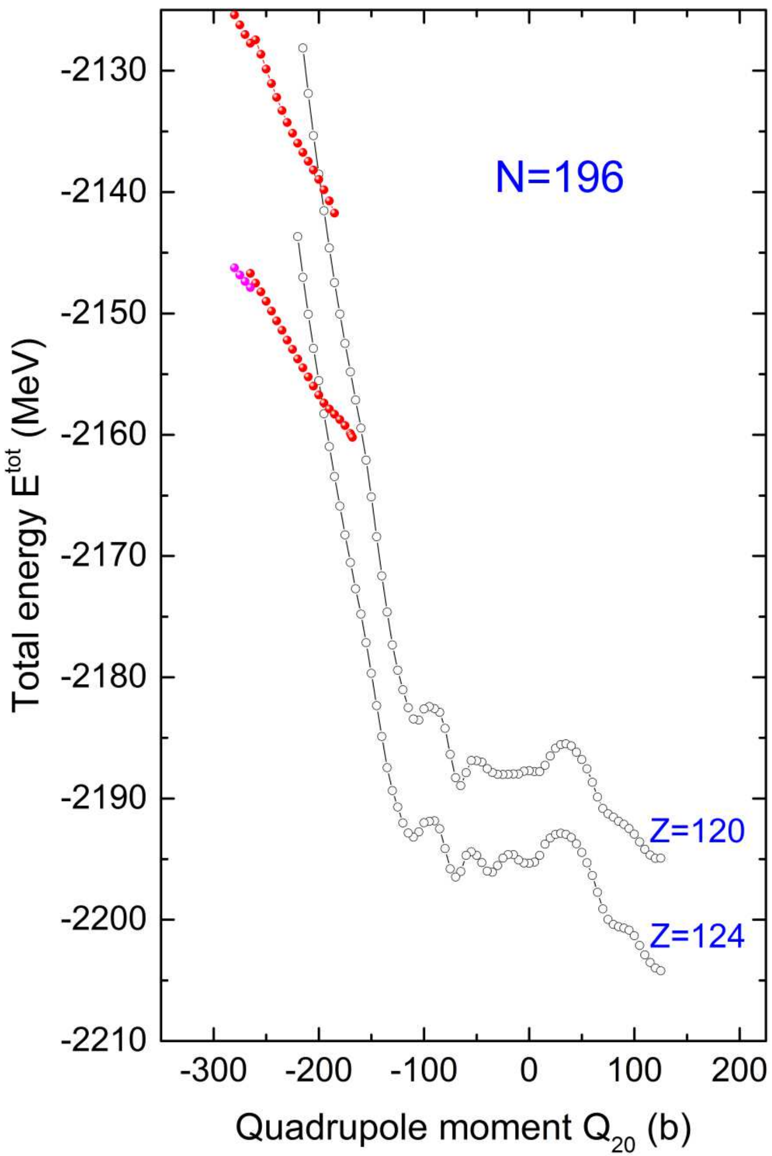

# Hiper-heavy isotones $N$=196

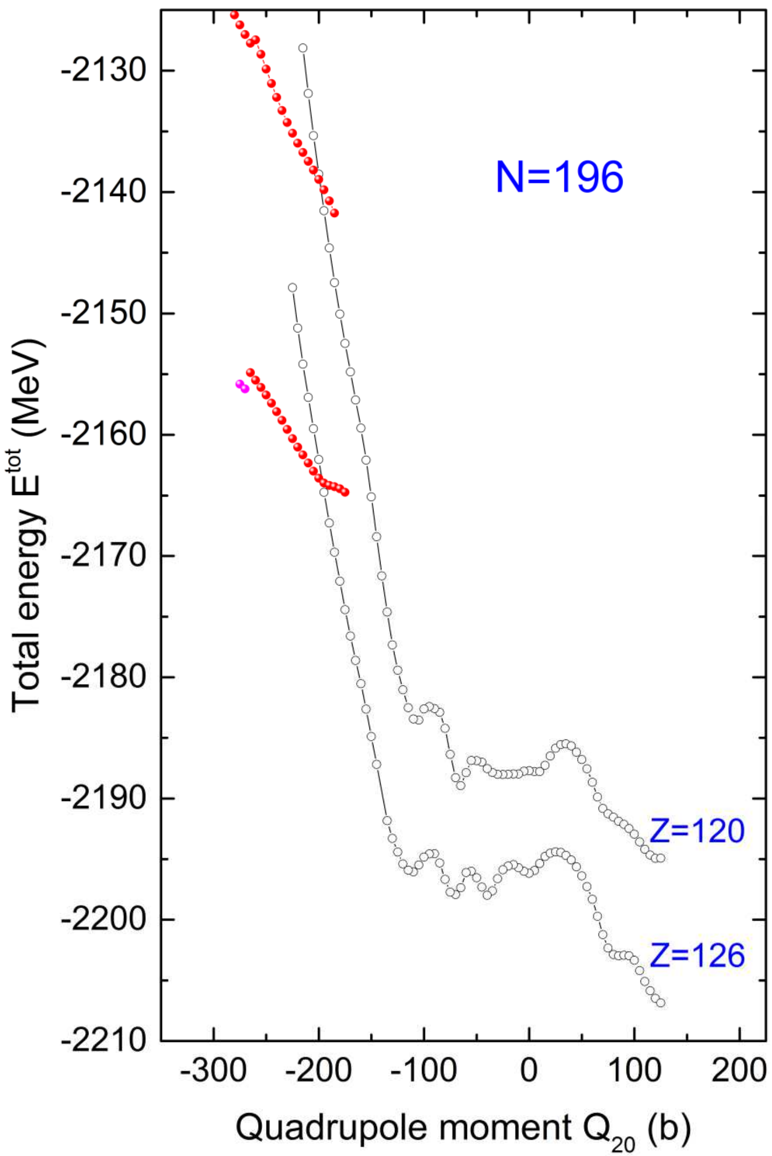

# Hiper-heavy isotones $N$=196

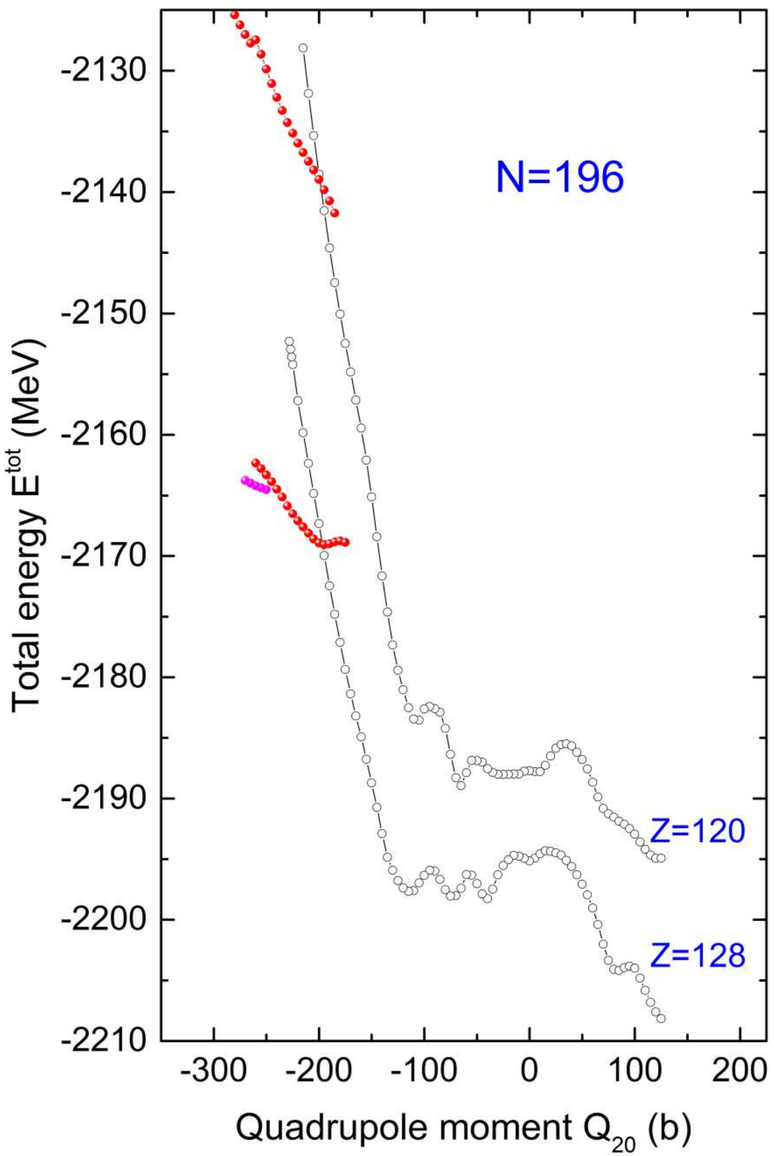

# Hiper-heavy isotones N=196

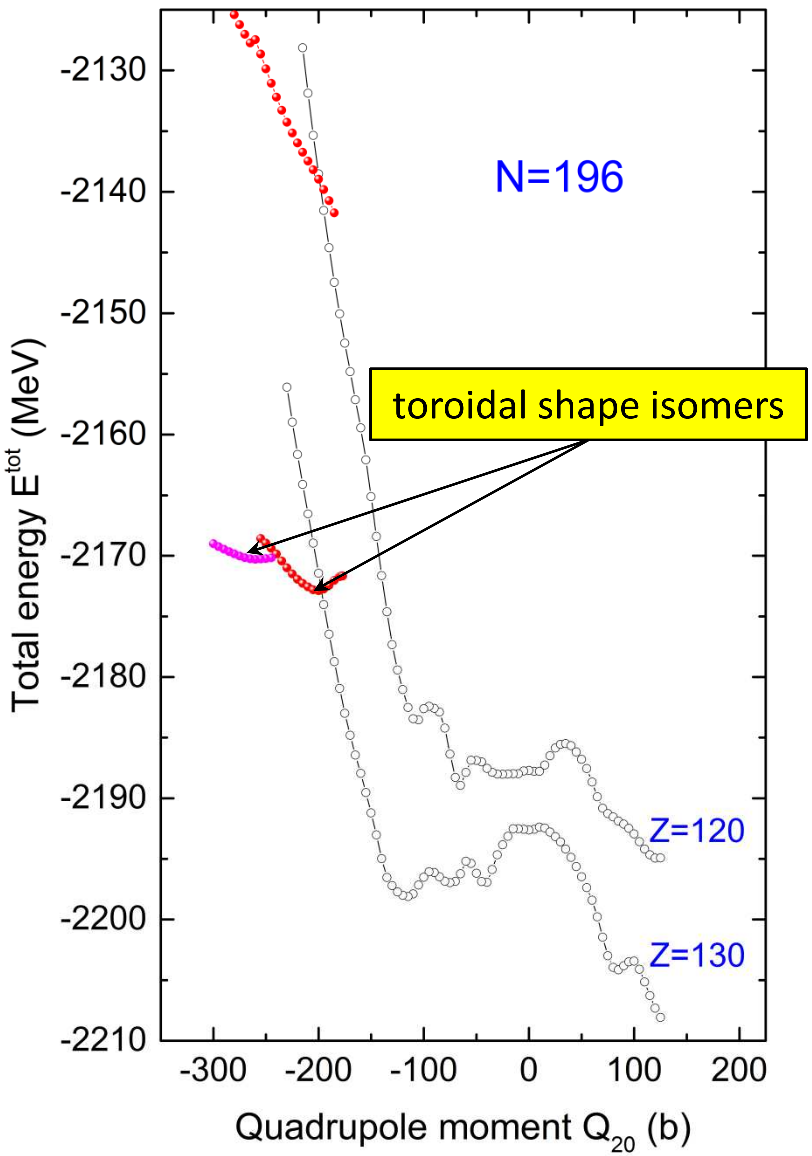

# Hiper-heavy isotones $N$=196

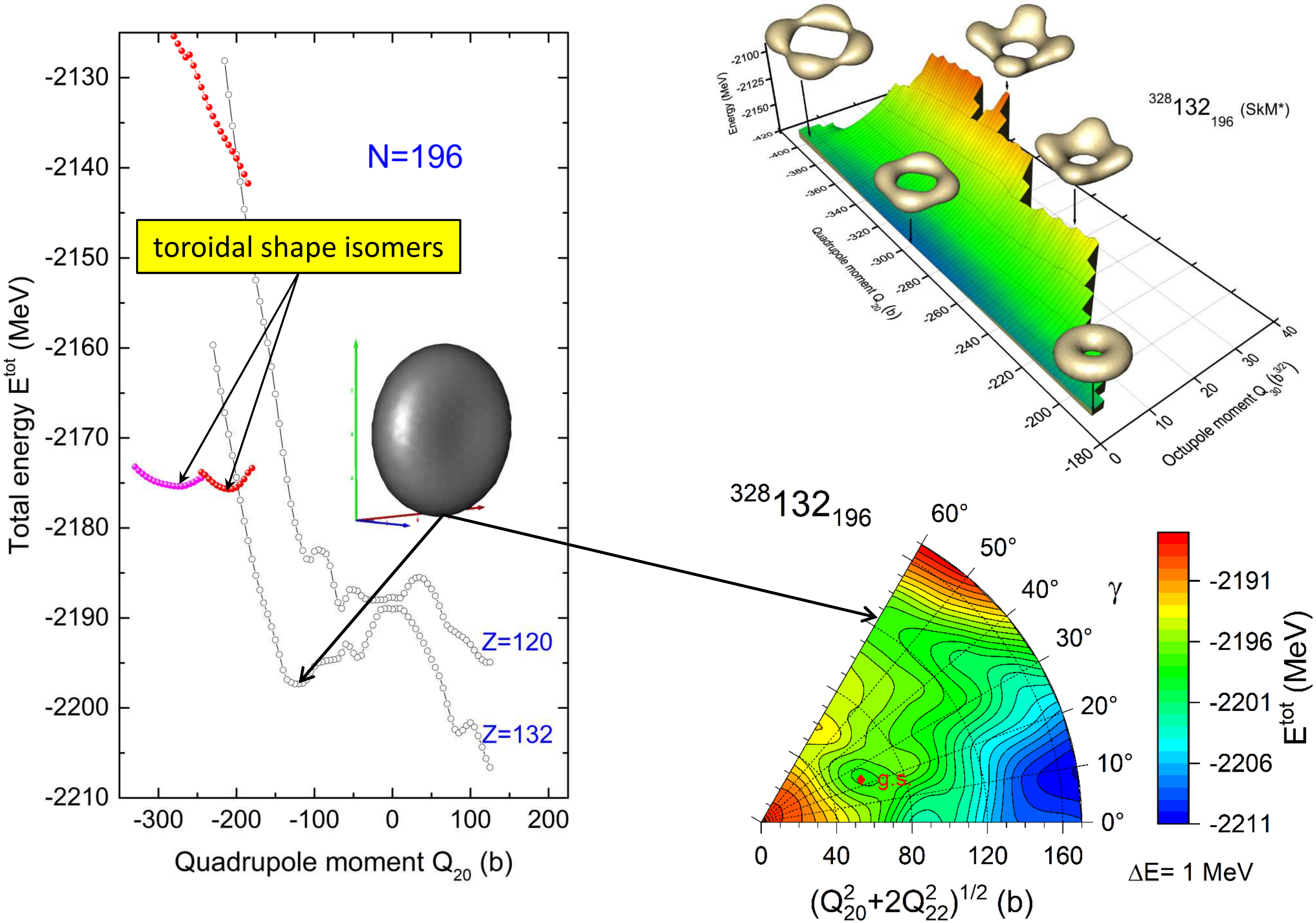

# Hiper-heavy isotones *N*=196 and isotopes *Z*=132

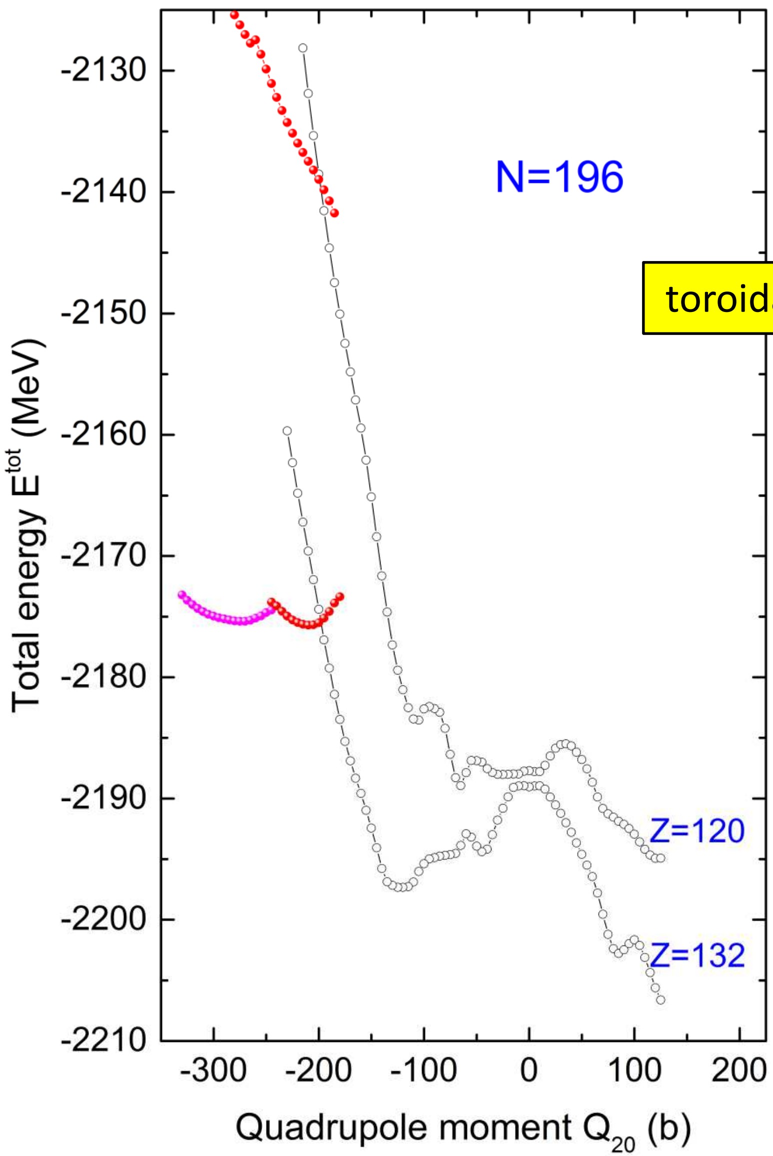


toroidal shape isomers

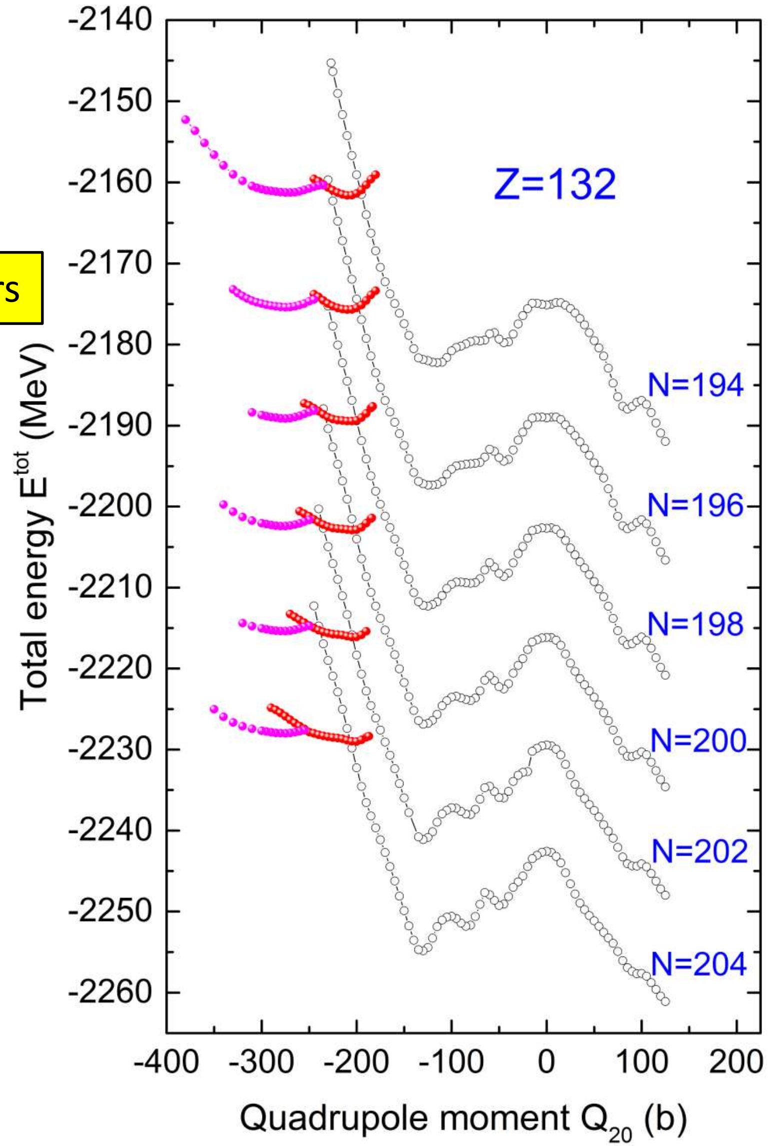

# Stability against triaxial distortion

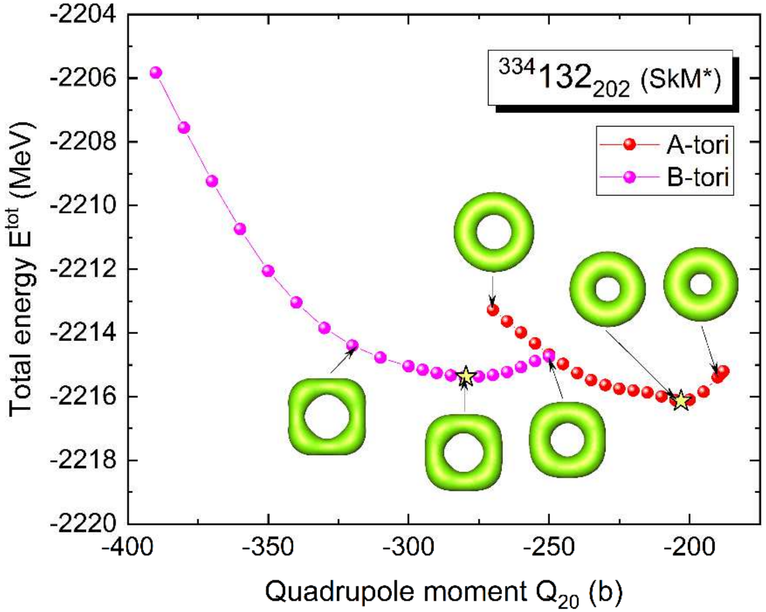


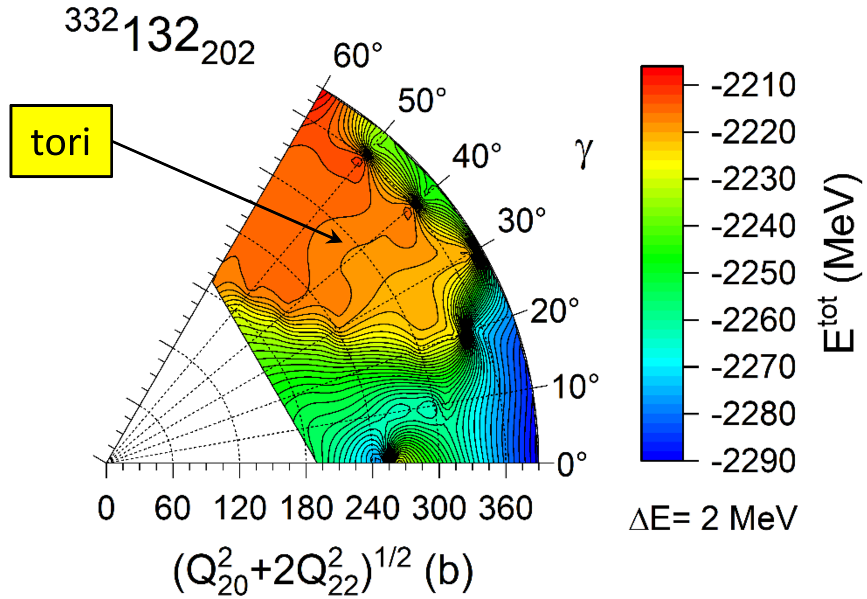


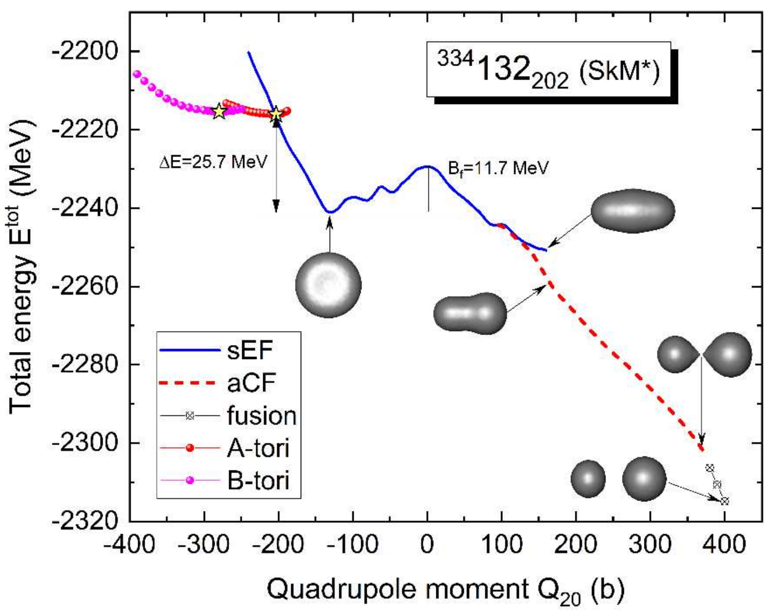


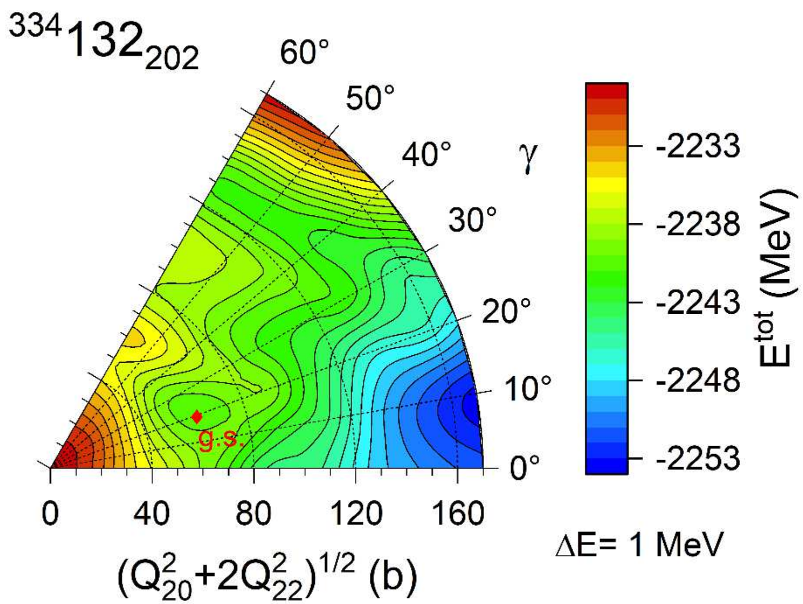

# The (β–γ) potential energy surface of e-e hiper-heavy *Z* = 132 and 134 isotopes

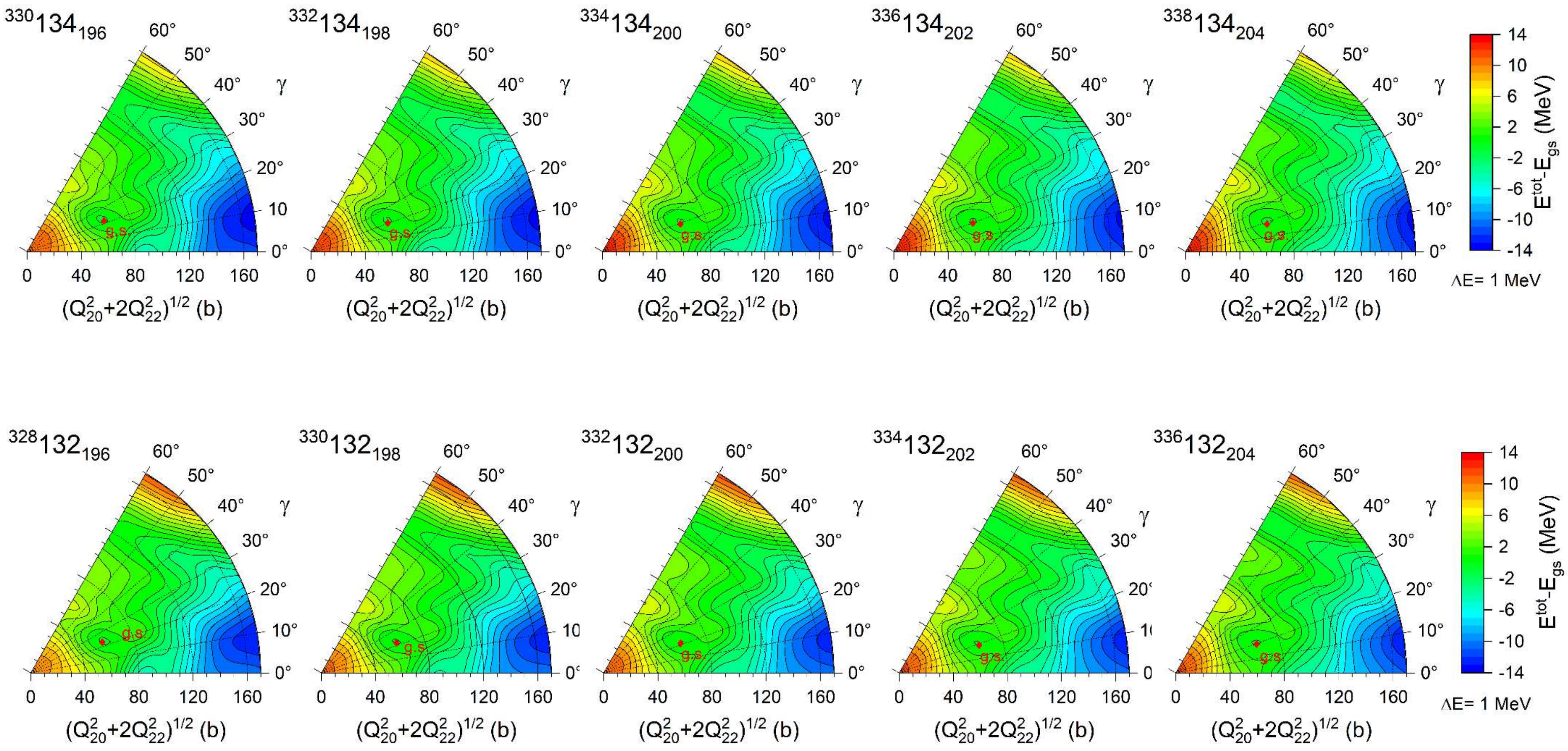


$$\beta = \sqrt{\frac{5}{16\pi}}\frac{4\pi}{3AR_0^2}\sqrt{Q_{20}^2 + 2Q_{22}^2} = \frac{\sqrt{5\pi}}{3r_0^2A^{5/3}}\sqrt{Q_{20}^2 + 2Q_{22}^2}\,, \quad \gamma = \tan^{-1}\frac{\sqrt{2}Q_{22}}{Q_{20}}\,.$$

# Possible mechanisms for the production of toroidal high-spin isomers (THSI) and toroidal vortex isomers

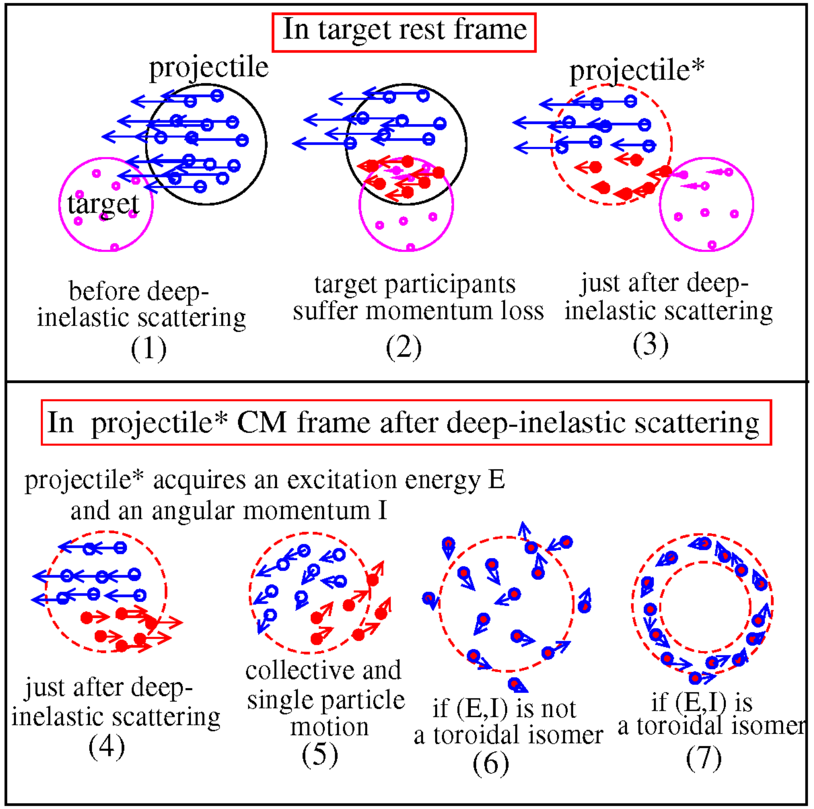


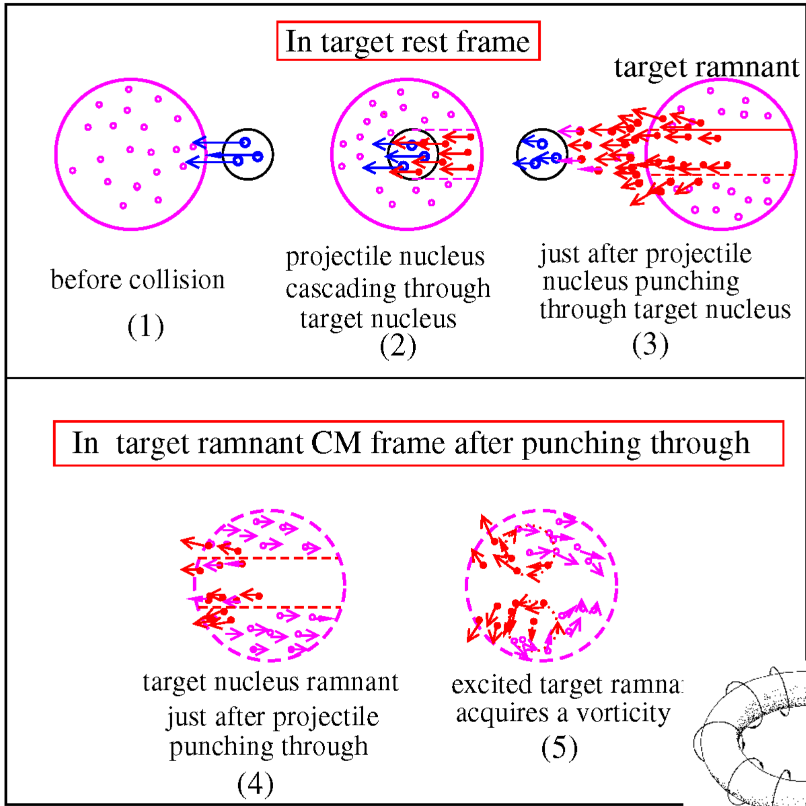


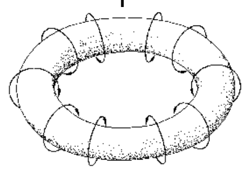

A) Production of a toroidal high-spin isomer by <u>deep-inelastic scattering</u>

B) Production of a toroidal vortex nucleus by <u>punching through a target nucleus</u>

C) Production of light-mass toroidal isomers by <u>elastic scattering</u> – time projection chambers (TPCs) of noble gases under a high voltage

**Evidence for high excitation energy resonances in the 7 alpha disassembly of $^{28}$Si**

X. G. Cao,[1,2] E. J. Kim,[2,3] K. Schmidt,[4,2] K. Hagel,[2] M. Barbui,[2] J. Gauthier,[2] S. Wuenschel,[2] G. Giuliani,[2,5] M. R. D. Rodriguez,[2,6] S. Kowalski,[4] H. Zheng,[2,5] M. Huang,[2,7] A. Bonasera,[2,5] R. Wada,[2] G. Q. Zhang,[1,2] C. Y. Wong,[8] A. Staszczak,[9] Z. X. Ren,[10] Y. K. Wang,[10] S. Q. Zhang,[10] J. Meng,[10,11] and J. B. Natowitz[2]

[1] *Shanghai Institute of Applied Physics, Chinese Academy of Sciences, Shanghai 201800, China*
[2] *Cyclotron Institute, Texas A&M University, College Station, Texas 77843*
[3] *Division of Science Education, Chonbuk National University, 567 Baekje-daero Deokjin-gu,Jeonju 54896, Korea*
[4] *Institute of Physics, University of Silesia, 40-007 Katowice, Poland.*
[5] *Laboratori Nazionali del Sud, INFN, via Santa Sofia, 62, 95123 Catania, Italy*
[6] *Instituto de Física, Universidade de São Paulo, Caixa Postal 66318, CEP 05389-970, São Paulo, SP, Brazil*
[7] *College of Physics and Electronics Information, Inner Mongolia University for Nationalities, Tongliao, 028000, China*
[8] *Physics Division, Oak Ridge National Laboratory, Oak Ridge, USA*
[9] *Institute of Physics, Maria Curie-Skłodowska University, Lublin, Poland*
[10] *State Key Laboratory of Nuclear Physics and Technology, School of Physics, Peking University, Beijing 100871, China*
[11] *Yukawa Institute for Theoretical Physics, Kyoto University, Kyoto 606-8502, Japan*

(Dated: October 2, 2018)

The excitation function for the 7 alpha de-excitation of $^{28}$Si nuclei excited to high excitation energies in the collisions of 35 MeV/nucleon $^{28}$Si with $^{12}$C reveals resonance structures that may indicate the population of toroidal high-spin isomers such as those predicted by a number of recent theoretical calculations. This interpretation is supported by extended theoretical analyses.

PACS numbers: 25.70.Pq
Keywords: Intermediate energy heavy ion reactions, Clusters

arXiv:1801.07366v2 [nucl-ex]

The experiment was performed at Texas A&M University Cyclotron Institute. A 35 MeV/nucleon $^{28}$Si beam produced by the K500 superconducting cyclotron impinged on a $^{12}$C target.

The smallest energy of detected alpha in 7alpha events is about 3.3 MeV in the lab frame. Thresholds are similar for other alpha conjugate exit channels. Using the AMD+GEMINI simulation analysis before and after experimental filtering, we can estimate the detection efficiencies for 7 alpha events: 0.108. The detected event numbers of 6 alphas, 7 alphas and 8 alphas are 24849, 6467, and 840, respectively. The ratio between them is: 1 : 0.26 : 0.03.

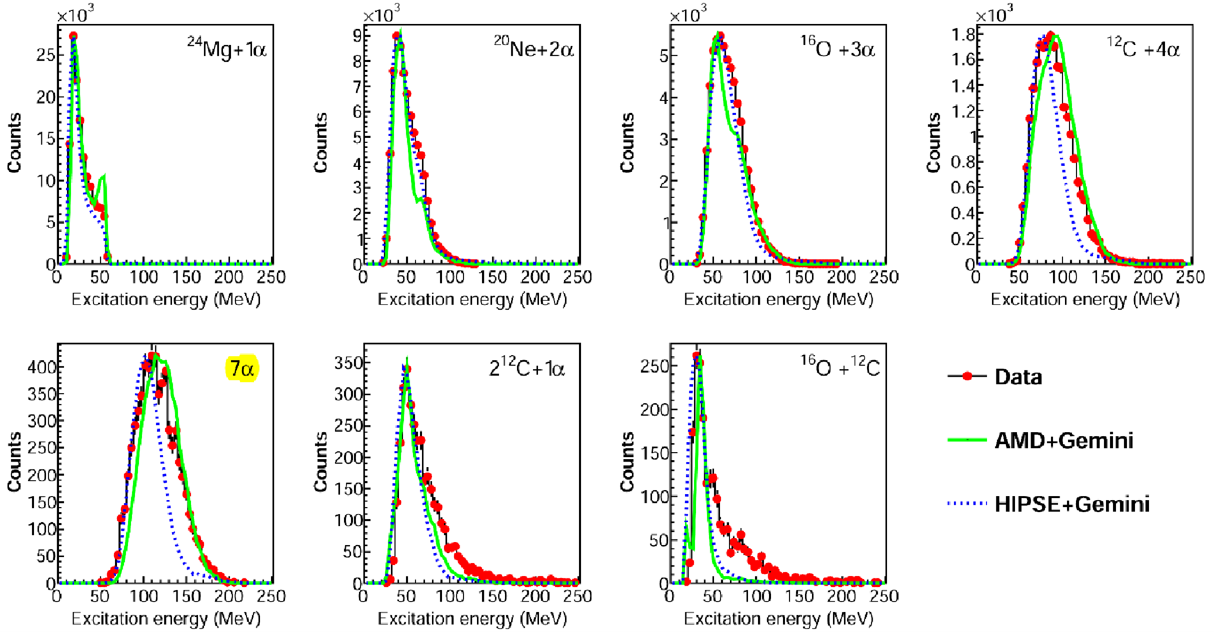


FIG. 1: Excitation functions for the alpha conjugate exit channels in the de-excitation of $^{28}$Si. The shapes of the experimental data are compared with results of both AMD and HIPSE calculations.

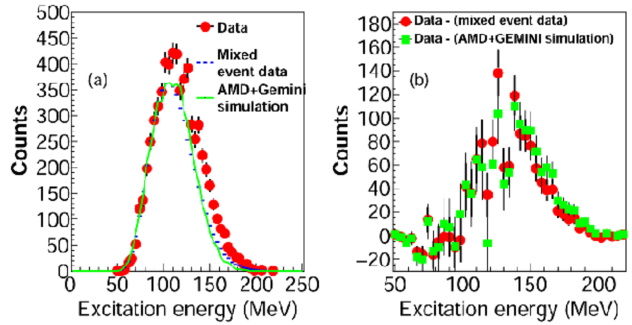


FIG. 2: Excitation energy distribution leading to observed 7-alpha events. Left panel-the data are represented by a solid black line. An uncorrelated spectrum derived from event mixing is represented by a long dashed line. The filtered result from an AMD-GEMINI calculation is indicated by the dashed and dotted line (see text). The last two are normalized to the experimental spectrum at the lower edge of the spectrum. On the right the differences between the experimental spectrum and the others are presented. Relative to the uncorrelated background derived from the experiment the statistical significance of the difference peak at 114 MeV is 5.3$\sigma$, at 126 MeV is 8.0$\sigma$ and at 138 MeV is 7.2$\sigma$. See text

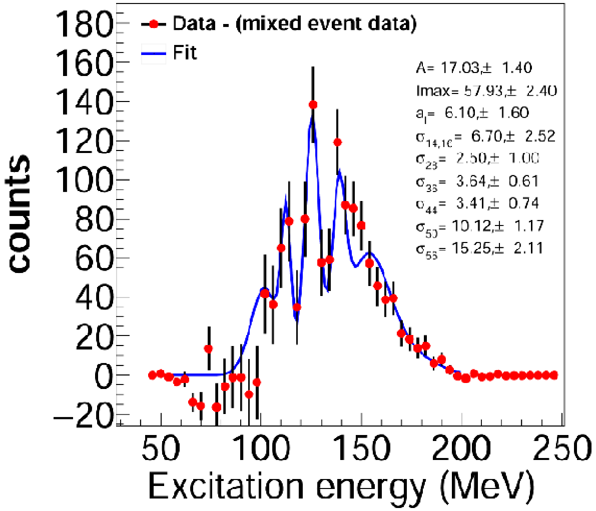


FIG. 4: The experimental (correlated data) - (mixed event data) (in solid points) are compared with the results of semi-empirical formula (4) containing the signature of the toroidal high-spin isomers as primary ingredients (in solid curve) with the list of extracted widths and other parameters.

**Table 1**
Properties of high-spin toroidal isomers at their local energy minima in $28 \leqslant A \leqslant 52$.

| | $I/\hbar$ | $Q_{20}$ (b) | $\hbar\omega$ (MeV) | $E^*$ (MeV) | $R$ (fm) | $d$ (fm) | $R/d$ | $\rho_{max}$ (fm$^{-3}$) |
|---|---|---|---|---|---|---|---|---|
| $^{28}$Si | 44 | −5.86 | 2.8 | 143.18 | 4.33 | 1.45 | 2.99 | 0.119 |
| $^{32}$S | 48 | −8.22 | 1.9 | 153.87 | 4.87 | 1.42 | 3.43 | 0.122 |
| | 66 | −10.51 | 2.2 | 193.35 | 5.57 | 1.40 | 3.98 | 0.108 |
| $^{36}$Ar | 56 | −11.31 | 1.7 | 168.03 | 5.44 | 1.40 | 3.88 | 0.125 |
| | 72 | −13.73 | 1.85 | 198.63 | 6.04 | 1.39 | 4.34 | 0.113 |
| | 92 | −16.78 | 2.0 | 238.56 | 6.73 | 1.37 | 4.91 | 0.103 |
| $^{40}$Ca | 60 | −14.96 | 1.5 | 178.36 | 5.97 | 1.40 | 4.26 | 0.126 |
| | 82 | −17.61 | 1.9 | 214.23 | 6.51 | 1.39 | 4.68 | 0.117 |
| $^{44}$Ti | 68 | −19.57 | 1.2 | 195.46 | 6.55 | 1.39 | 4.71 | 0.128 |
| | 88 | −22.27 | 1.4 | 223.09 | 7.01 | 1.38 | 5.08 | 0.120 |
| | 112 | −25.76 | 1.6 | 260.24 | 7.56 | 1.37 | 5.52 | 0.113 |
| $^{48}$Cr | 72 | −25.08 | 1.2 | 207.12 | 7.12 | 1.38 | 5.16 | 0.128 |
| | 98 | −28.00 | 1.4 | 239.26 | 7.54 | 1.37 | 5.50 | 0.122 |
| | 120 | −30.55 | 1.43 | 271.02 | 7.90 | 1.36 | 5.81 | 0.118 |
| $^{52}$Fe | 52 | −29.24 | 0.8 | 202.86 | 7.39 | 1.38 | 5.35 | 0.134 |
| | 80 | −31.43 | 0.95 | 227.54 | 7.68 | 1.38 | 5.56 | 0.130 |
| | 104 | −33.54 | 1.3 | 252.65 | 7.94 | 1.37 | 5.79 | 0.126 |
| | 132 | −35.62 | 1.5 | 288.91 | 8.20 | 1.36 | 6.03 | 0.123 |

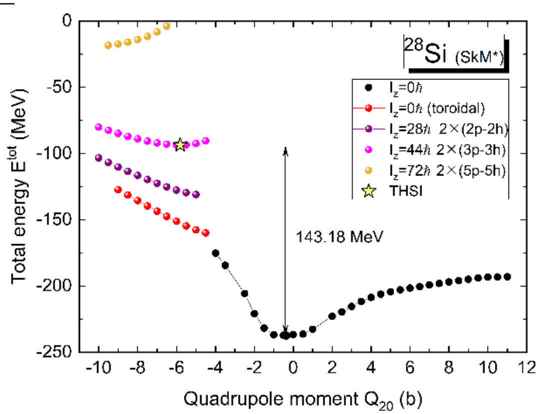


A. S. and C. Y. Wong, Phys. Lett. B 738, 401 (2014).

# Streszczenie

Badania z wykorzystaniem średnio-polowych modeli samo-zgodnych (z nałożonymi więzami na masowy moment kwadrupolowy $Q_{20}$) wskazują, że niezależnie od masy jądra atomowego (z liczbą masową $A > 12$) obserwujemy uniwersalny proces ewolucji kształtu jąder. W miarę jak w obliczeniach zmniejsza się zadana wartość momentu kwadrupolowego ($Q_{20} < 0$) elipsoidalne jądro osiąga kształt dysku (deformacja *oblate*), by następnie stać się dyskiem dwustronnie wklęsłym (podobnym do krwinki czerwonej - erytrocytu). Dalsza ewolucja kształtu jądra prowadzi do rozkładu materii jądrowej w postaci torusa.

Należy podkreślić uniwersalny charakter zaobserwowanego (jak dotąd tylko teoretycznie) zjawiska:
dla dostatecznie dużych wartości deformacji *oblate* "toroidalne rozwiązania" w samo-zgodnych obliczeniach średnio-polowych pojawiają się zarówno dla jąder lekkich jak i najcięższych.

Toroidalne jądro jest układem silnie wzbudzonym i niestabilnym. Okazuje się jednak, że wzbudzenia cząstka-dziura nukleonów, w przypadku takich jąder, prowadzić mogą do izomerycznych (metastabilnych) stanów wysoko-spinowych.

Dodatkowym czynnikiem stabilizującym jądra w kształcie torusa jest liczba atomowa $Z$. W przypadku, gdy liczba protonów w jądrze osiąga wartość $Z = 132$ (hipotetyczne jądra *hiper-ciężkie*) toroidalne rozwiązania tworzą lokalne płaskie minimum, które wskazuje na możliwość istnienia toroidalnego stanu izomerycznego (bez wzbudzeń cząstka-dziura nukleonów).

# Collaboration

## Cheuk-Yin Wong (ORNL), Amelia Kosior (UMCS)

- A. S. and C. Y. Wong, *Toroidal super-heavy nuclei in Skyrme-Hartree-Fock approach*, Acta Phys. Polonica B 40, 1001 (2009).
- A. S. and C. Y. Wong, *A region of high-spin toroidal isomers*, Phys. Lett. B 738, 401 (2014).
- A. S. and C. Y. Wong, *Particle-hole nature of the light high-spin toroidal isomers*, Acta Phys. Polonica B 46, 675 (2015).
- A. S. and C. Y. Wong, *Toroidal high-spin isomers in light nuclei with N≠Z*, Phys. Scr. 90, 114006 (2015).
- A. S. and C. Y. Wong, *Theoretical studies of possible toroidal high-spin isomers in the light-mass region*, EPJ Web of Conferences 117, 04008 (2016).
- A. Kosior, A. S., and C. Y. Wong, *Toroidal nuclear matter distributions of superheavy nuclei from constrained Skyrme-HFB calculations*, Acta Phys. Polonica B Proc. Suppl. 10, 249 (2017).
- A. S., C. Y. Wong, and A. Kosior, *Toroidal high-spin isomers in the nucleus* $^{304}120$, Phys. Rev. C 95, 054315 (2017).
- A. Kosior, A. S., and C. Y. Wong, *Properties of superheavy isotopes Z = 120 and isotones N = 184 within the Skyrme–HFB model*, Acta Phys. Polonica B Proc. Suppl. 11, 167 (2018).
- C. Y. Wong and A. S., *Shells in a toroidal nucleus in the intermediate-mass region*, Phys. Rev. C 98, 034316 (2018).

Dziękuję za poświęconą uwagę!

# Light *N*=*Z* toroidal nuclei in constrained SkM*-HFB model

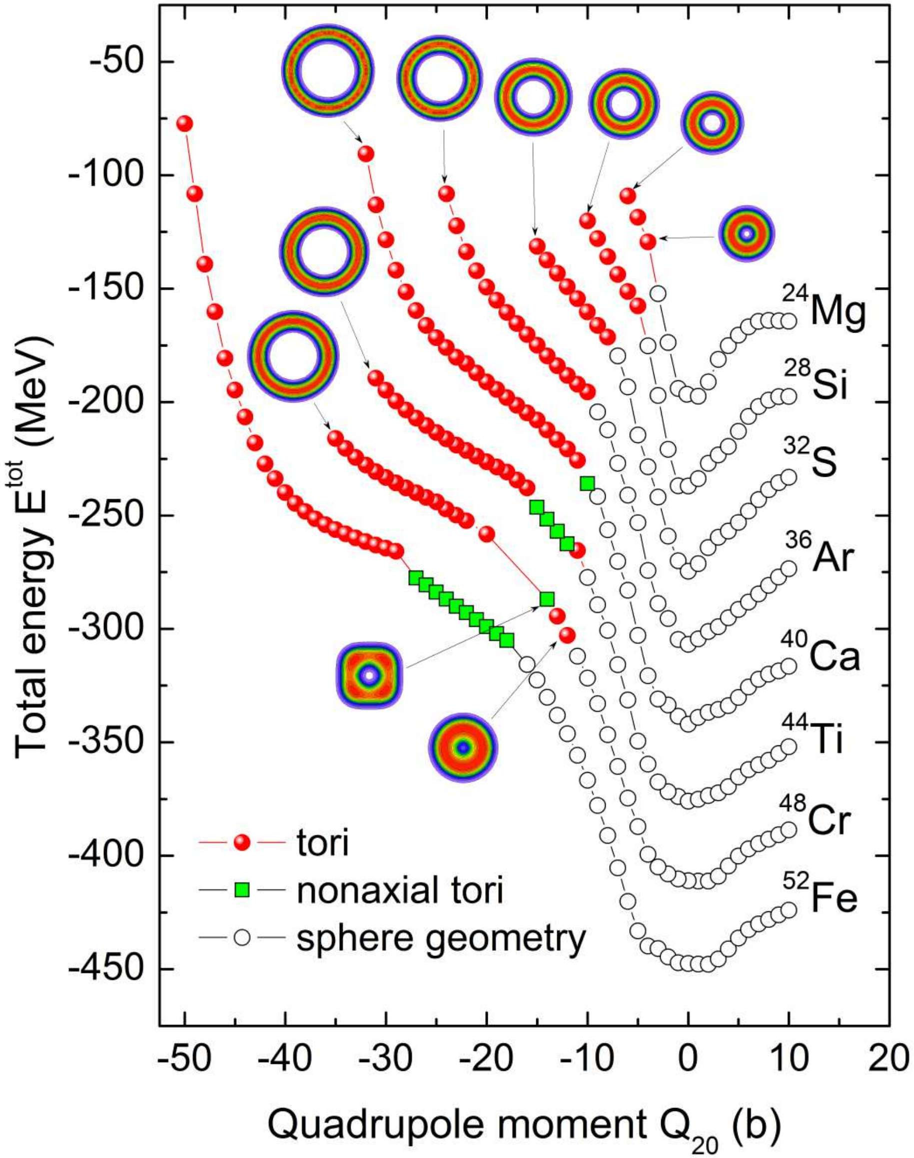


A. S., C. Y. Wong, arXiv: 1038777

# Toroidal nuclei in cranked SkM*-HF model

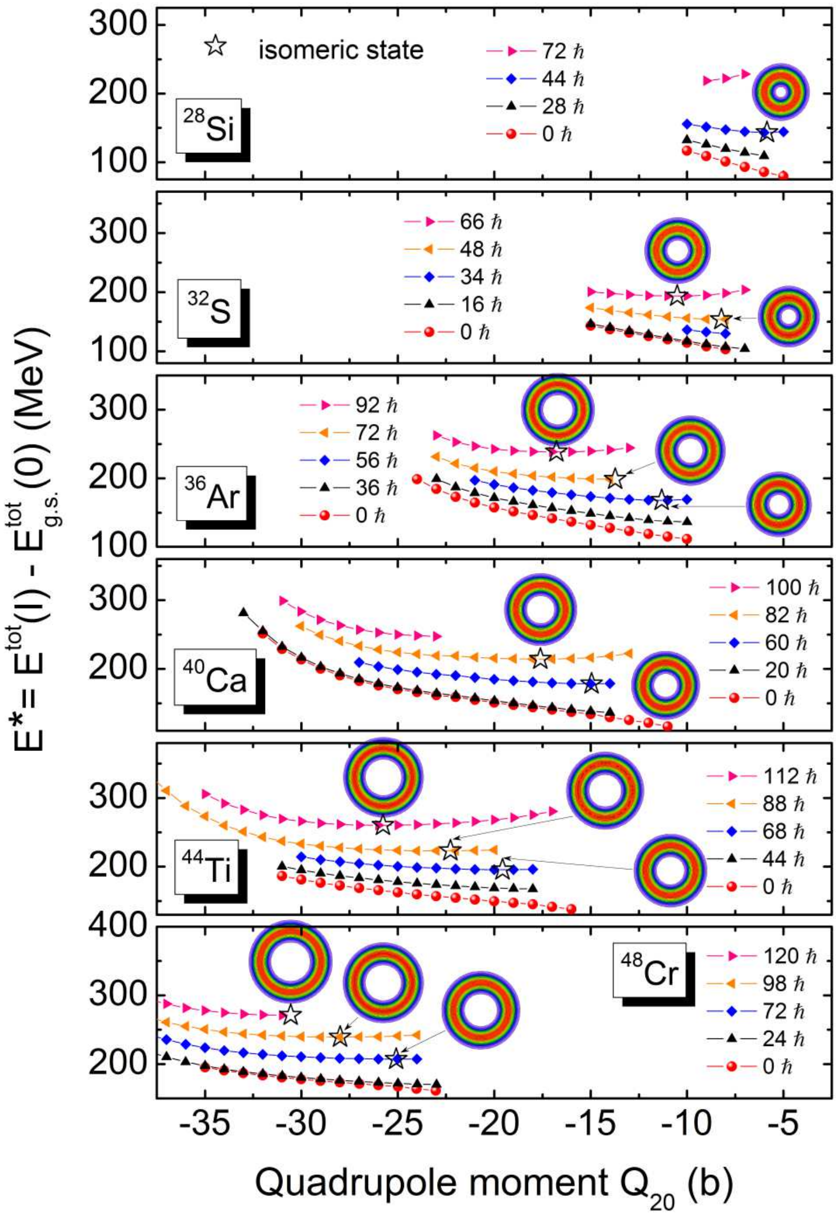


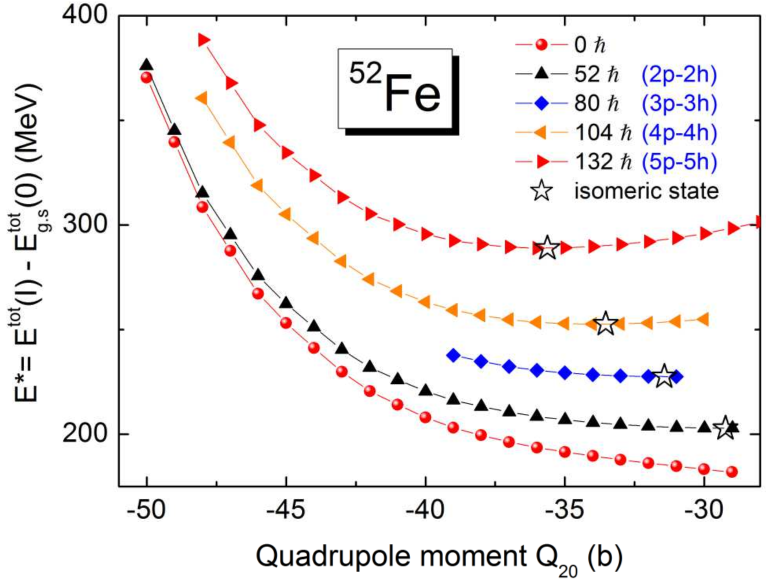


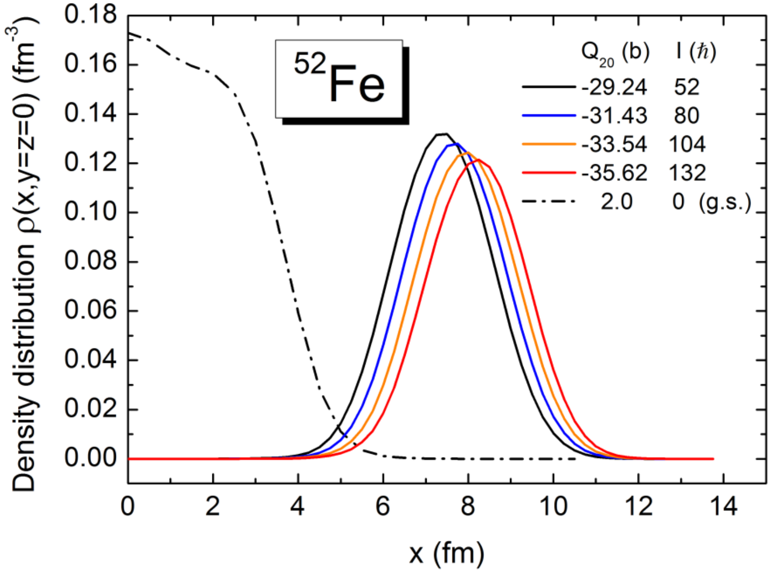


arXiv: 1038777

# High-K toroidal isomers in 28≤A≤52

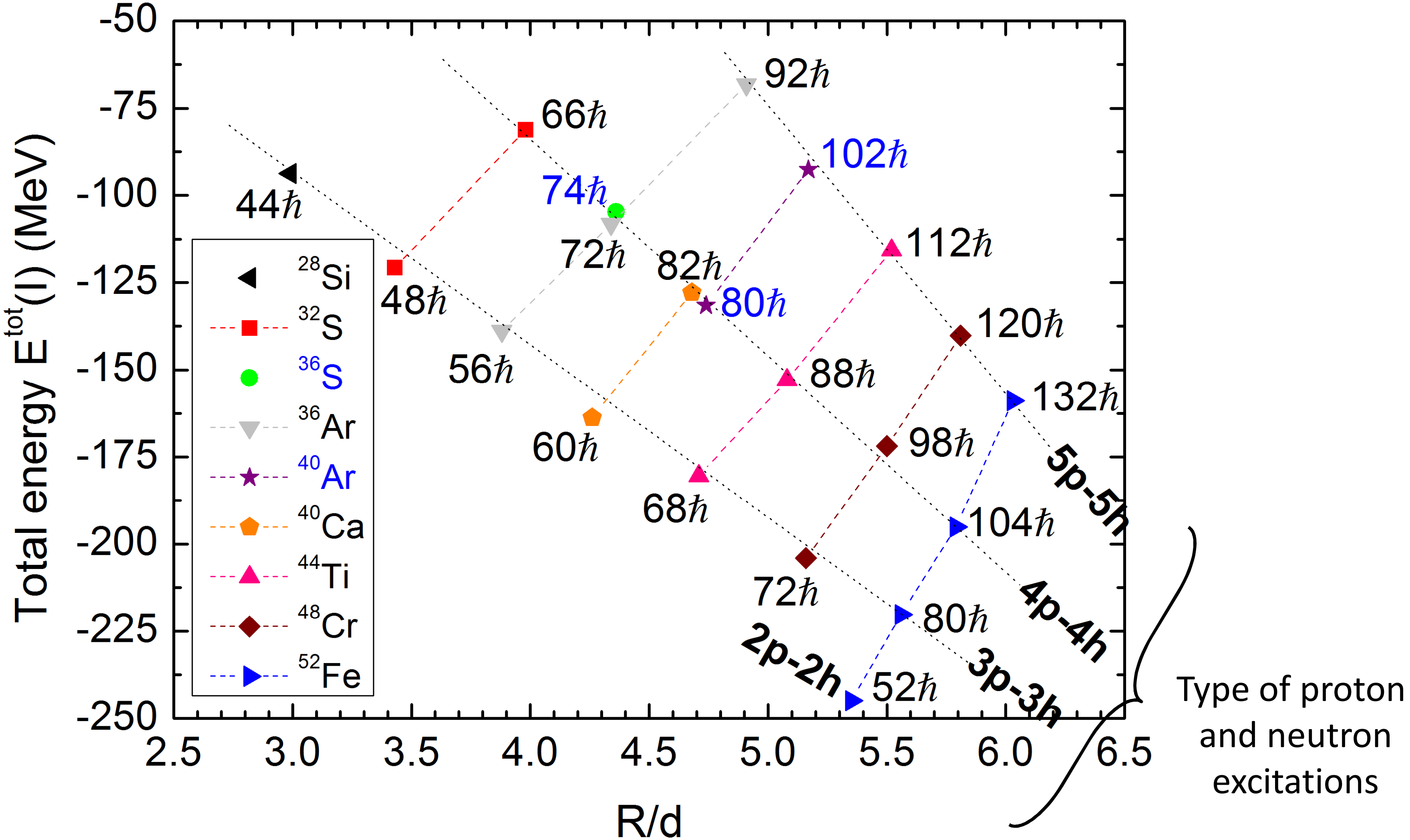

# Light rotating toroidal nuclei in HF-cranking model

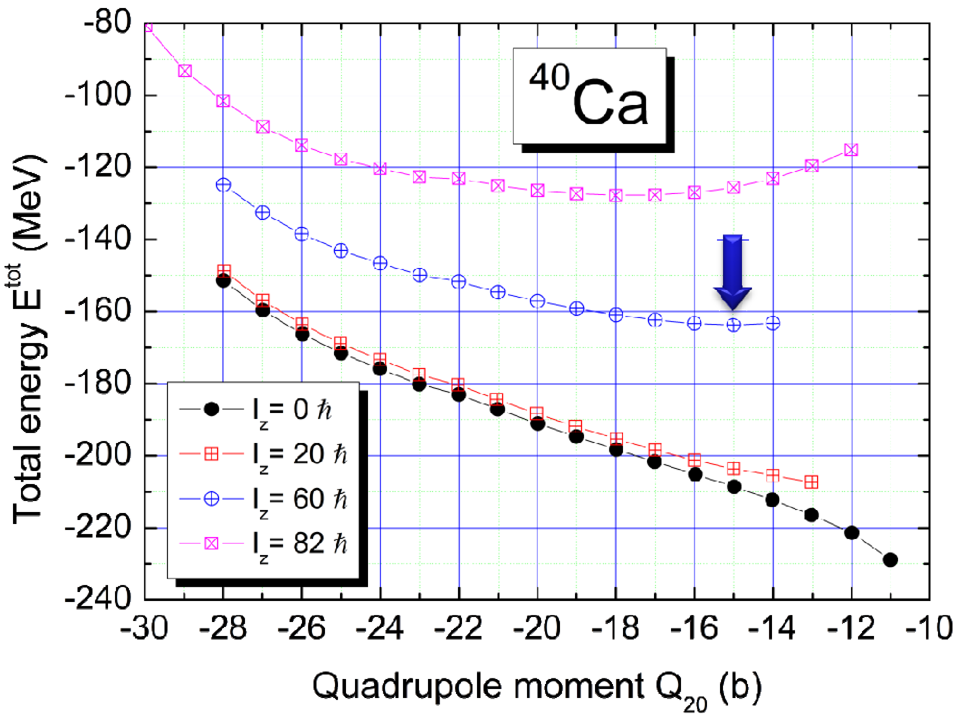


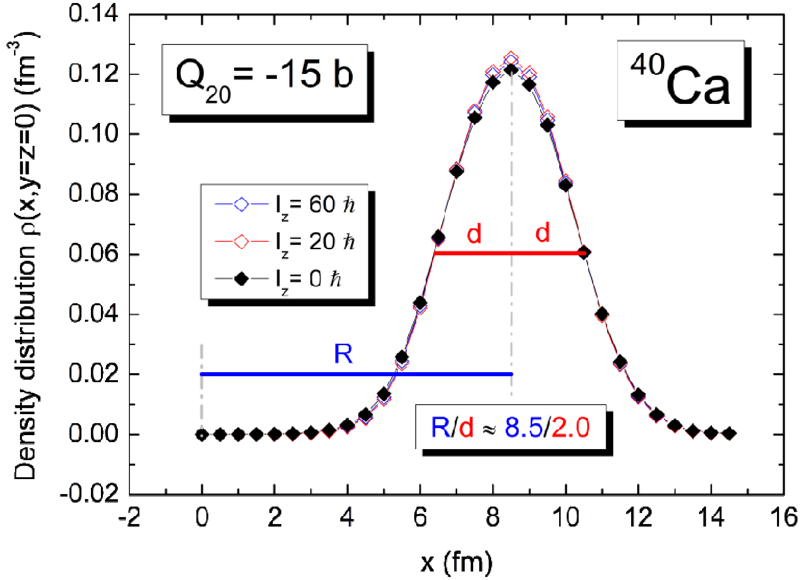


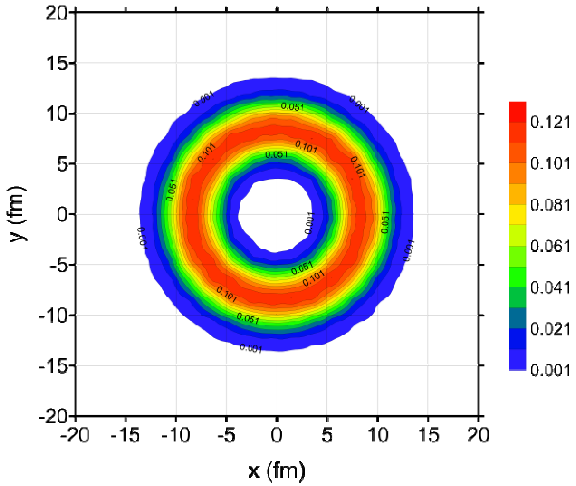


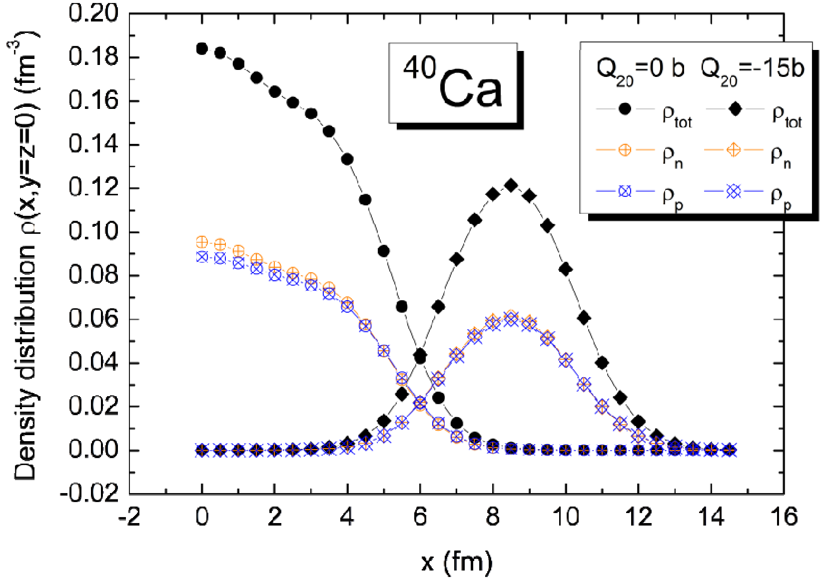

# Toroidal high-K isomers as a possible source of energy!?

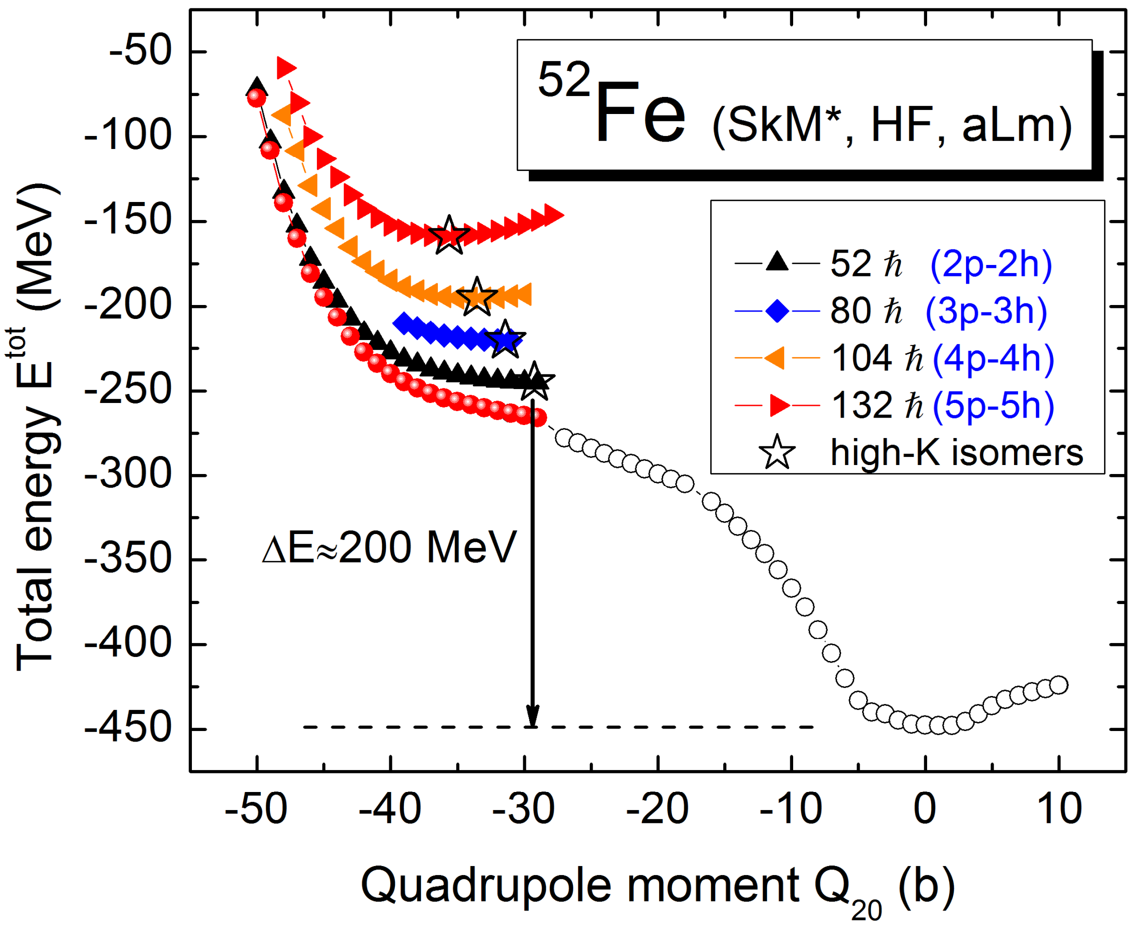

# Moment of inertia

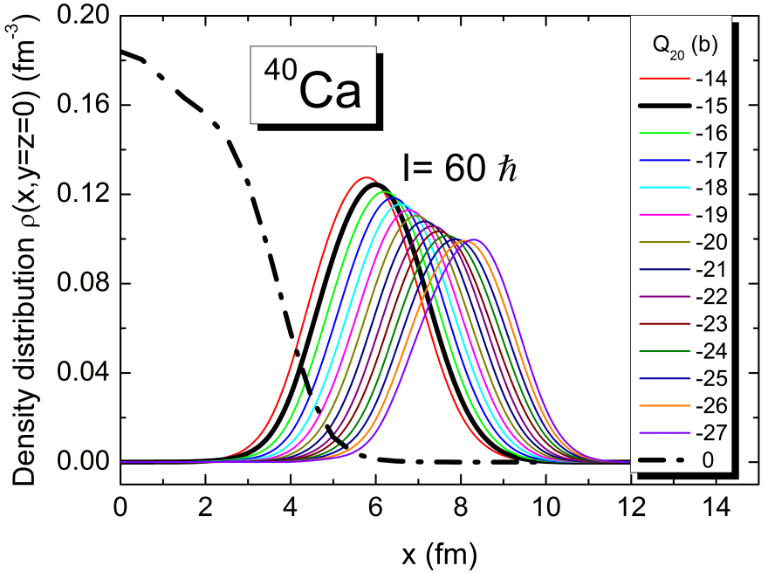


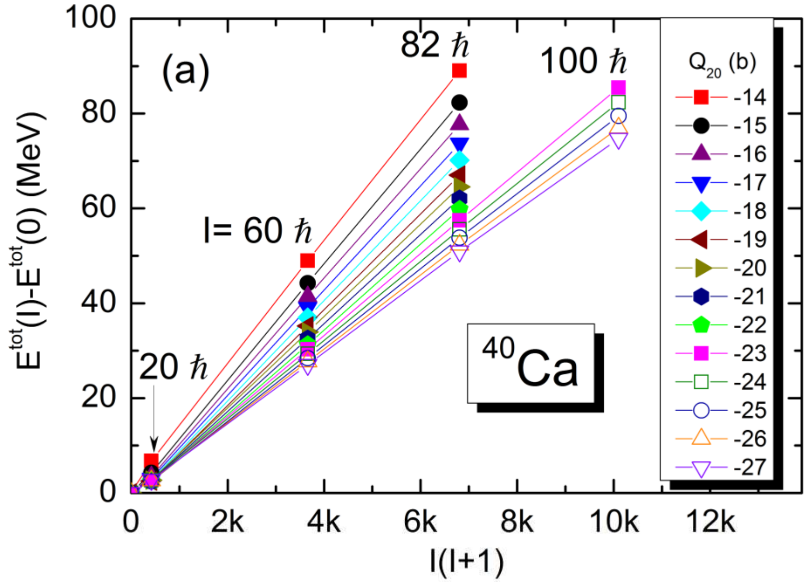


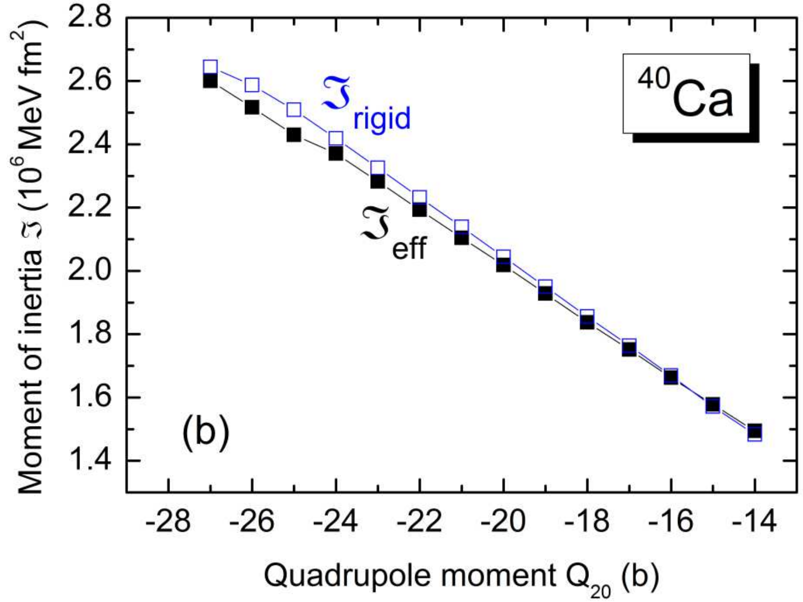


An effective moment of inertia:

$$E^{tot}(I) = E^{tot}(0) + \frac{\hbar^2}{2\Im_{eff}} I(I+1).$$

The toroidal density can be parametrized as

$$\rho(r,z) = \rho_{\max} \exp\{-[(r-R)^2 + z^2]/\sigma^2\},$$

$$\sigma = d\big/\sqrt{\ln 2}, \quad d \equiv \tfrac{1}{2}\mathrm{FWHM},$$

and the rigid-body moment of inertia is

$$\Im_{rigid} = m_N 2\pi^2 R^2 \sigma^2 \rho_{\max}(R^2 + \tfrac{3}{2}\sigma^2).$$

arXiv: 1038777

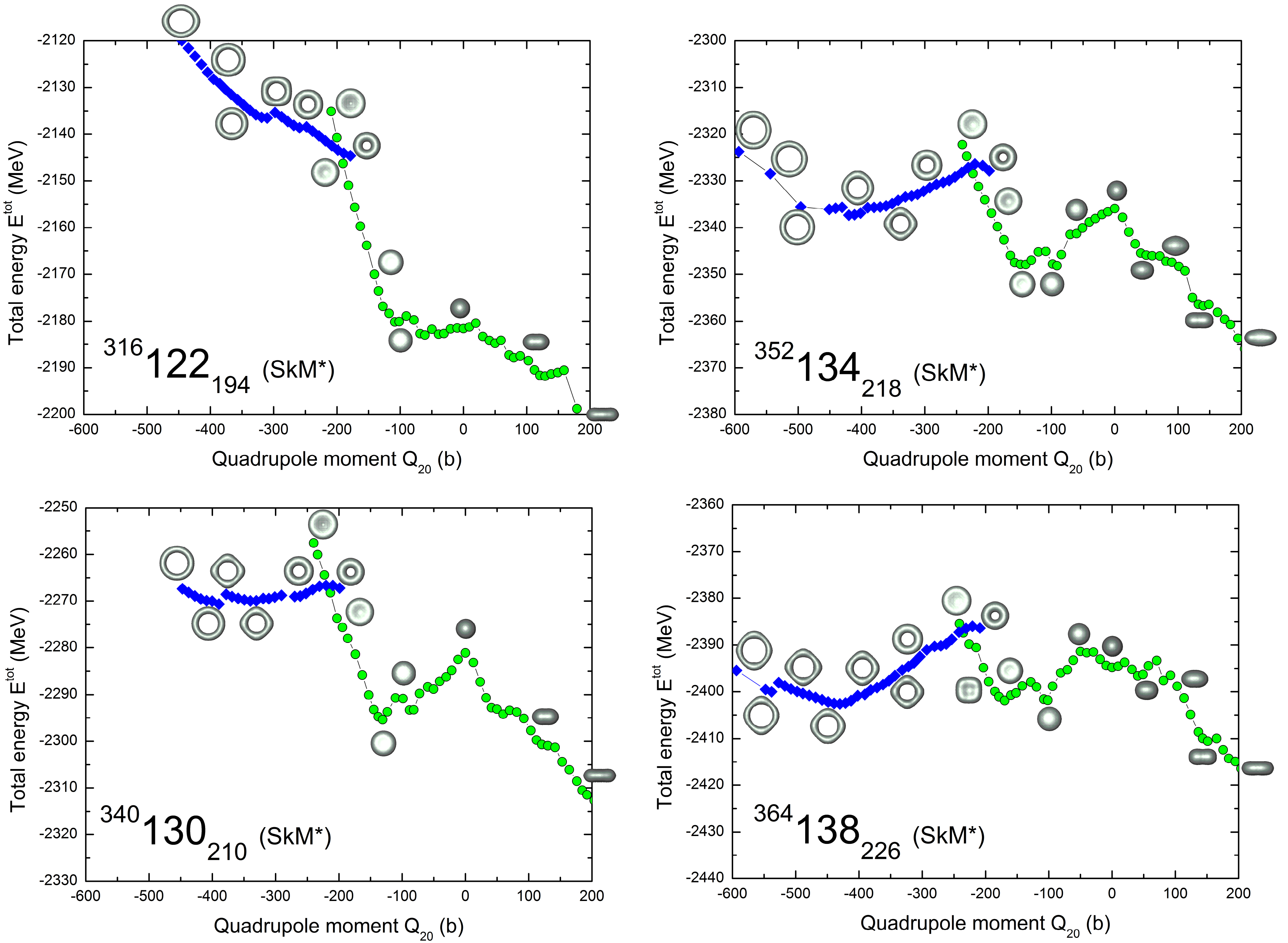

Total energy $E^{tot}$ (MeV)
Quadrupole moment $Q_{20}$ (b)
$^{316}122_{194}$ (SkM*)
$^{352}134_{218}$ (SkM*)
$^{340}130_{210}$ (SkM*)
$^{364}138_{226}$ (SkM*)

## Conclusions

Our studies show that the toroidal (genus 1) form of the nuclear density distribution is not an exceptional phenomenon, but a regular characteristic of strongly oblate deformed heavy and super-heavy nuclei.

The doughnut shaped nuclei are not the exception, but the rule!
(in this region of deformations)

The genus 1 and genus 0 total energy minima become closer in energy
With increasing the atomic number Z and the mass number A.

For Z=138 and A=364 the toroidal equilibrium begins to be a global minimum.

The toroidal solutions are more stable against β-decay than the genus 0 solutions.

A. S. and C. Y. Wong, Acta Phys. Pol. B **40**, 753 (2009).

# SkM*-CHFB model

The symmetry unrestricted code HFODD [1] and an augmented Lagrangian method [2] were used to solve constrained HFB equations with SkM* Skyrme force [3] in the p-h channel and a density dependent mixed pairing [4, 5] interaction in the p-p channel.

The stretched harmonic oscillator basis of HFODD was composed of states having not more than $N_0$ = 26 quanta in either of the Cartesian directions, and not more than 1140 states in total.

| | SkM* | SLy4 | Units/Comments |
|---|---|---|---|
| $t_0$ | -2645.0 | -2488.913 | MeV fm$^3$ |
| $t_1$ | 410.0 | 486.818 | MeV fm$^5$ |
| $t_2$ | -135.0 | -546.395 | MeV fm$^5$ |
| $t_3$ | 15595.0 | 13777.0 | MeV fm$^{3+\alpha}$ |
| $x_0$ | 0.09 | 0.834 | - |
| $x_1$ | 0.0 | -0.344 | - |
| $x_2$ | 0.0 | -1.000 | - |
| $x_3$ | 0.0 | 1.354 | - |
| $1/\alpha$ | 6.0 | 6.0 | - |
| $W_0$ | 120.0 | 123.0 | MeV fm$^5$ |
| $C_t^J$ | 0.0 | 0.0 | (spin-orbit tensor term, $\mathbb{J}^2$) |
| $\rho_{st}$ | 0.16 | 0.16 | fm$^{-3}$ |
| $\beta$ | 1.0 | 1.0 | - |
| $E_{cut}$ | 60 | - | MeV (HFB) |
| $E_{cut}$ | - | N or Z | (no. of s.p. states, BCS) |
| $V^1$ | 0.5 | 1 | (0.5-mixed, 1-surface pairing) |
| $V_n^0$ | -268.9 | -842.0 | MeV fm$^3$ |
| $V_p^0$ | -332.5 | -1020.0 | MeV fm$^3$ |


[1] N. Schunck *et al.*, Comput. Phys. Comm. **216**, 145 (2017).

[2] A. Staszczak, M. Stoitsov, A. Baran, and W. Nazarewicz, Eur. J. Phys. A **46**, 85 (2010).

[3] J. Bartel *et al.*, Nucl. Phys. A **386**, 79 (1982).

[4] J. Dobaczewski, W. Nazarewicz, and M. V. Stoitsov, Eur. J. Phys. A **15**, 21 (2002).

[5] A. Staszczak, A. Baran, J. Dobaczewski, and W. Nazarewicz, Phys. Rev. C **80**, 014309 (2009).

# The total energy in the Skyrme-HF/HFB model

$$\boxed{\begin{aligned} E^{tot} &\equiv \langle \Phi_{HF} | \hat{H} | \Phi_{HF} \rangle \geqslant E_{g.s.} \\ &= \int \mathrm{d}^3\boldsymbol{r} \, \left[ \mathcal{E}_{kin} + \mathcal{E}_{Sk} + \mathcal{E}_{Coul}^{dir} + \mathcal{E}_{Coul}^{ex} + \mathcal{E}_{pair} \right] + E_{corr}, \end{aligned}}$$

$$\mathcal{E}_{kin} = \frac{\hbar^2}{2m} \tau_0(\boldsymbol{r}),$$

kinetic energy density

$$\mathcal{E}_{Coul}^{dir} = \tfrac{1}{2} e^2 \rho_p(\boldsymbol{r}) \int \mathrm{d}^3\boldsymbol{r}' \, \frac{\rho_p(\boldsymbol{r}')}{|\, \boldsymbol{r} - \boldsymbol{r}' \,|},$$

direct Coulomb en. density

$$\mathcal{E}_{Coul}^{ex} = -\tfrac{3}{4} e^2 \left( \tfrac{3}{\pi} \right)^{1/3} \rho_p^{4/3}(\boldsymbol{r})$$

exchange Coulomb en. density
(in the Slater approx.)

$$\mathcal{E}_{pair} = \sum_{q=p,n} \frac{V_q^0}{4} \left[ 1 - V^1 \left( \frac{\rho_0(\boldsymbol{r})}{\rho_{st}} \right)^{\beta} \right] \tilde{\rho}_q^2(\boldsymbol{r}),$$

Isovector pairing en. density

$V^1 = 0,\ 1,\ \mathrm{or}\ 1/2$ for *volume-*, *surface-*, or *mix-*type pairing

$\rho_{st} = 0.16\,\mathrm{fm}^{-3}$ ; ½$_q$(r ) - pairing density for protons and neutrons.

# The equality-constrained prpblem (ECP)

$$\begin{cases} \min\limits_{\bar{\rho}} E^{tot}[\bar{\boldsymbol{\rho}}] \\ \text{subject to:} \quad \sum\limits_{q=p,n} \langle \Phi(\bar{\boldsymbol{\rho}}) | \hat{N}_q | \Phi(\bar{\boldsymbol{\rho}}) \rangle = N_q, \\ \qquad\qquad\qquad \sum\limits_{\lambda\mu} \langle \Phi(\bar{\boldsymbol{\rho}}) | \hat{Q}_{\lambda\mu} | \Phi(\bar{\boldsymbol{\rho}}) \rangle = Q_{\lambda\mu}, \end{cases}$$

$$\begin{aligned} E^{tot}[\bar{\boldsymbol{\rho}}] &\equiv E^{tot}\left[\rho, \tau, \mathbb{J}; \boldsymbol{s}, \boldsymbol{T}, \boldsymbol{j}, \boldsymbol{F}; \tilde{\rho}\right] \\ &= \int \mathrm{d}^3\boldsymbol{r} \left(\mathcal{E}_{kin}(\boldsymbol{r}) + \mathcal{E}_{Sk}(\boldsymbol{r}) + \mathcal{E}^{dir}_{Coul}(\boldsymbol{r}) + \mathcal{E}^{ex}_{Coul}(\boldsymbol{r}) + \mathcal{E}_{pair}(\boldsymbol{r})\right) + E_{corr} \end{aligned}$$

*an objective function*

The Skyrme EDF in the case of even-even nuclei (time-reversal symmetry)

$$\begin{aligned} \mathcal{E}^{even}_{Sk}(\boldsymbol{r}) &= \sum_{t=0,1} \left( C^{\rho}_t[\rho_0]\rho_t^2 + C^{\Delta\rho}_t \rho_t \Delta\rho_t + C^{\tau}_t \rho_t \tau_t + \cancel{C^J_t \mathbb{J}^2_t} \right) \quad \text{(central terms)} \\ &+ \sum_{t=0,1} \left( C^{\nabla J}_t \rho_t \boldsymbol{\nabla} \cdot \boldsymbol{J}_t \right), \quad \text{(spin-orbit term)} \end{aligned}$$

# HFODD: the self-consistent symmetries

- time-reversal $\hat{T}$
- parity $\hat{P}$
- x-, y-, z-signature $\hat{R}_{x,y,z} = \exp(-i\pi \hat{J}_{x,y,z})$
- x-, y-, z-simplex $\hat{S}_{x,y,z} = \hat{P}\hat{R}_{x,y,z}$
- x-, y-, z-simplex*T $\hat{S}^{T}_{x,y,z} = \hat{T}\hat{S}_{x,y,z}$

| $\hat{T}$ | $\hat{S}_y$ | $\hat{S}^T_y$ |
|---|---|---|
| $\hat{P}$ | $\hat{S}_y$ | $\hat{R}_y$ |
| $\hat{R}_y$ | $\hat{S}^T_x$ | $\hat{S}^T_z$ |
| 1 | 1 | 1 |
| 1 | 0 | 0 |
| 0 | 1 | 0 |
| 0 | 0 | 1 |
| 0 | 0 | 0 |

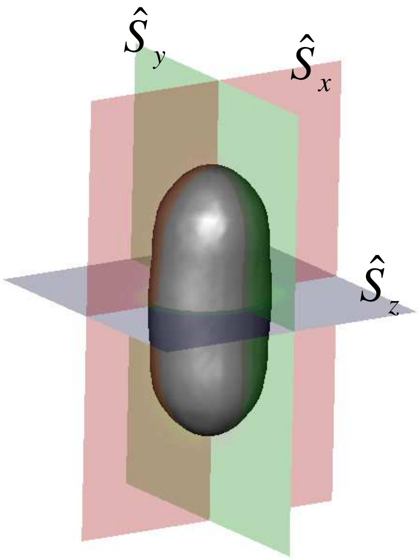


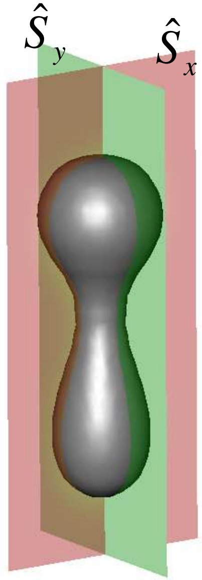


$$\hat{S}_y = 1 \Rightarrow Q_{\lambda\mu} = \langle \hat{Q}_{\lambda\mu} \rangle \in \mathbb{R}$$

$$Q_{\lambda-odd,\mu} \neq 0 \;\; only\;\; for \;\; \hat{P} = 0$$